scientific reports

Check for updates

OPEN

Establishing FDA-approved oncology drugs as GPR176 inhibitor through homology modelling, molecular docking, MMGBSA, DFT, and molecular dynamics simulation

Felix Oluwasegun Ishabiyi[1,2,8]✉, Haruna Isiyaku Umar[8,9]✉, Tanmoy Dutta[3], Okoyenta Celestina Onyinye[4,8], Olusola Daniel Damola[5,8], Leyla Budagova[7,8], Denekew Temesgen[13]✉, Mohammed Bourhia[10], Ridwan Opeyemi Bello[6], Esmael M. Alyami[11,14], Mona Alsolami[11] & Omar A. Almohammed[12]

The GPR176 protein is a cell membrane protein implicated in human diseases, especially cancers. Numerous studies have highlighted its overexpression, which is considered a major driver of tumorigenesis. Reducing its overexpression has been shown by many studies to be a viable pharmacological strategy for cancer therapy, prompting this study to search for drug molecules from existing FDA-approved drugs. We performed homology modeling of the GPR176 protein to obtain its 3D structure, conducted docking simulations of FDA-approved drugs retrieved from ReDO_DB to identify compounds with strong binding affinities, and carried out density functional theory quantum calculations and molecular dynamic simulations to assess stability and compactness. Additionally, pharmacokinetic profiling and drug-likeness analyses were performed to identify molecules capable of inhibiting and potentially deorphanizing GPR176. We identified Fostamatinib and Ticagrelor as both compounds exhibited binding affinities of -11.503 kcal/mol and – 11.882 kcal/mol, which indicates that both compounds effectively interact with the protein; they both had minimal deviations from their natural states as the RMSD values of 0.35 and 0.45 characterize their stability profile; energy gap of -0.1327 eV and – 0.1371 eV, which illuminates their reactivity to the protein and favorable pharmacokinetic profiles compared to the control, Vismodegib. This leads to the identification of Fostamatinib and Ticagrelor as potential inhibitors of the protein, and thus, we recommend further experimental studies to validate these findings.

Keywords GRP176, Homology modelling, FDA-aproved drugs, Oncology, Computational drug design

The GPR176 belongs to the seven-transmembrane G-Protein Coupled Receptors (GPCRs) and it is involved in tumorigenesis[1]. The GPCRs are the largest group of membrane proteins and are implicated in diverse physiological processes[2]. Structurally, the GPR176 is made up of three extracellular and intercellular loops, with

[1]Faculty of Pharmacy, University of Ibadan, Ibadan, Nigeria. [2]Drug Discovery and Development, Herbal Medicine Development and Regulatory Science, African Centre of Excellence for Drug Research, University of Lagos, Lagos, Nigeria. [3]Department of Chemistry, JIS College of Engineering, Nadia, Kalyani 741235, West Bengal, India. [4]Biochemistry and Nutrition Department, Nigerian Institute of Medical Research, Yaba, Lagos, Nigeria. [5]Department of Biochemistry, Kwara State University, Malete, Nigeria. [6]Faculty of Medicine, University of Queensland, Brisbane, Australia. [7]Department of Biology, Faculty of Science, Selcuk University, Konya, Turkey. [8]Computer-Aided Therapeutic Discovery and Design Laboratory, Akure, Nigeria. [9]Department of Biochemistry, Federal University of Technology, PMB 704, Akure, Nigeria. [10]Swalife Biotech Ltd Unit 3D North Point House, North Point Business Park, Cork, Ireland. [11]Department of Biology, College of Science, King Khalid University, PO Box 960, Asir, Abha 61421, Saudi Arabia. [12]Department of Clinical Pharmacy, College of Pharmacy, King Saud University, Riyadh, Saudi Arabia. [13]Department of Biology, Bahir Dar University, P.O.Box 79, Bahir Dar, Ethiopia. [14]Research Centre for Advanced Materials Science (RCAMS), King Khalid University, Abha 61413, Saudi Arabia. ✉email: felixishabiyi@gmail.com; uhumar@futa.edu.ng; temesgenresearcher@gmail.com

the N-terminus located in the extracellular region, while the C-terminus is found on the cytosolic sites[3] (Fig. 1). Its basal activity is attributed to halting cAMP production, which results in its biological effects[3]. They are categorized as an important therapeutic target in diseases: they exhibit biological effects when stimulated by ligands[4]. A stimulation by either an endogenous or exogenous ligand prompts these proteins to initiate and mediate signaling cascades implicated in the normal physiological and pathological pathways, which corroborate their potential as viable therapeutic targets[5,6].

The GPCRs have been noted to be involved in several diseases[7]. Their involvement ranges from genetic disease[8], neurodegenerative[9], Psychiatric Disorders[10], inflammation[11], infectious[12], and in oncology[13]. They have been particularly elucidated to be a major driver of cancerous cells[14]. Studies have illuminated the GPR176 protein as druggable for anti-cancer chemotherapeutic development[15]. The protein was revealed to be involved in its clinical and pathological features in ovarian cancer due to the overexpression of its associated genes: N-cadherin, Zeb1, Snail, Twist1[16]. While in breast cancer, it was indicated to be a potential target for gene therapy as it aids tumor cell proliferation, suppressing anti-tumour activities of breast cancer cell lines[17]; the GPR176 is also implicated in Stomach Adenocarcinoma[18] and in colorectal cancer, the protein promotes cancer progression by recruiting the GNAS intracellularly via its transmembrane and inhibiting mitophagy by activating the cAMP/PKA/BNIP3L signaling pathway[19]. This study leverages the ability of this protein to mediate the pivotal pathways that catalyze tumorigenesis to identify new drug compounds for anti-cancer therapy.

The development of new bioactive compounds to inhibit the GPR176 would be burdensome: the resultant effect from the financial implications in the drug discovery and developmental processes[20–22]. As a result, we opted to identify new GPR176 inhibitors by evaluating already FDA-approved oncology drugs. The FDA-approved drugs are bioactive compounds that have been proven safe and certified by the Food and Drug Administration, and as such, can be used in patients living with the conditions for which they have been approved[23,24]. The ReDO_DB database houses several approved bioactive compounds for different types of cancers[25]. In this study, we sought to identify new inhibitors of the GPR176 by assessing their pharmacological activity using in silico techniques.

Deploying computational tools to augment the drug discovery process has been beneficial in the identification of new bioactive compounds[26,27]. One of the major ways it does this is by the virtual screening of thousands of compounds to identify new hits[2829],, which in turn compresses time in search for the same hits using the traditional approach[3031],. For this study,, we virtually screened the ReDO_DB, using the Vismodegib as a control, to identify the approved drugs with the utmost activity in reacting to the modelled three-dimensional structure of the GPR176, reconfirmed their binding strength by performing an Induced Fit Docking, to derive precise prediction of their binding strength to the protein, these compounds were subjected to the Molecular Mechanics Generalized Born Surface Area (MMGBSA), and to delineate their stability, flexibility, and robustness, the top two complexes were subjected to the Molecular Dynamics to illuminate more about these atomistic details. Importantly, it is worth noting that Vismodegib is used as a comparator to the GPR176 from the Smoothened (SMO), a 7-transmembrane protein. This results from the unavailability of established ligands for the GPR176, thus informing our control choice for this study.

To explore the therapeutic prospects of the selected ligands, we relied on a combination of in silico strategies. In modern drug discovery, computational methods such as molecular docking and molecular dynamics (MD) simulations serve as essential approaches for delineating the molecular principles of ligand–target recognition[32,33]. Docking enables the estimation of favorable binding orientations and affinities of small molecules within a receptor cavity, while MD simulations extend this prediction by monitoring the temporal stability and conformational adaptability of the complexes, thereby offering detailed insights into interaction dynamics and energetic profiles. Furthermore, density functional theory (DFT) calculations, specifically the evaluation

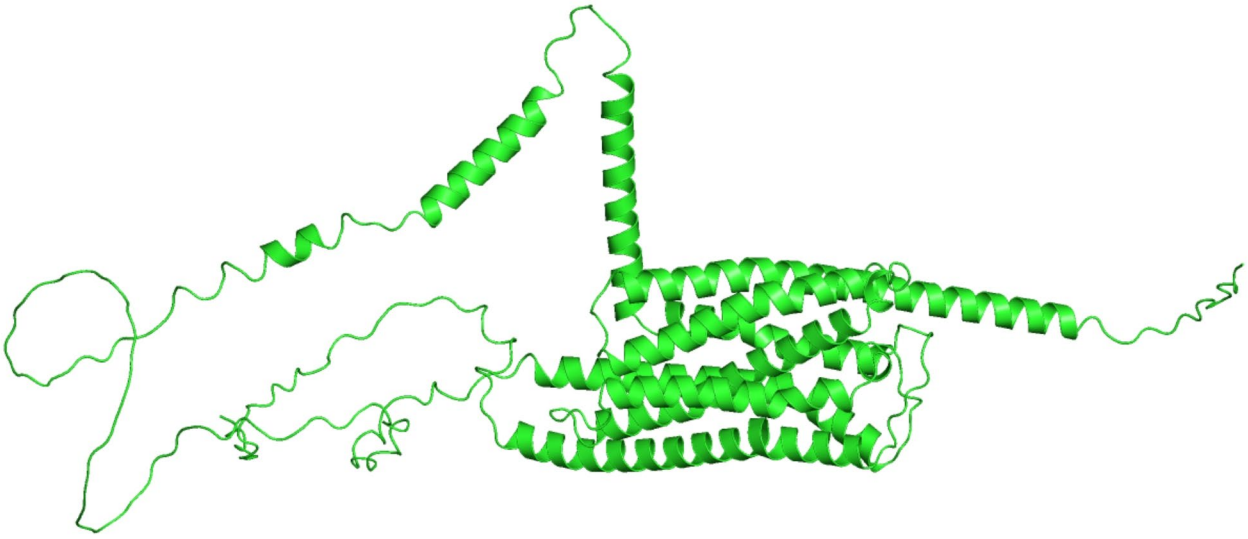

Fig. 1. GPR176 in cartoon representation.

of HOMO–LUMO gaps, Mulliken charge distribution[34], and global reactivity descriptors, provide a quantum-chemical perspective on the electronic structure and reactive tendencies of the ligands. Complementary to these methods, in silico absorption, distribution, metabolism, and excretion (ADME) assessments help determine the pharmacokinetic suitability of candidate molecules, reinforcing their potential as drug-like compounds[32].

Methodology

Homology modelling

The three-dimensional structure of GPR176 (305 amino acids) was successfully generated through homology modeling using the Swiss-Model (https://swissmodel.expasy.org). This was executed using the Alphafold server GRP176 (Q14439.1.A) with an identity of 100%, GMQE of 0.66, and coverage of 1. This server was deployed due to its template-driven refinement and efficient computational integration. The protein is in an inactive state. To assess the reliability and stereochemical quality of the modelled GPR176 structure, ProSA-web (https://prosa.services.came.sbg.ac.at/prosa.php) was employed. The ProSA Z-score for the model was − 1.79, which falls within the range of scores typically observed for native protein structures of similar size (~ 305 residues). Additionally, a Ramachandran plot was generated to evaluate the stereochemical quality of the protein backbone conformation. The majority of residues were located in the most favored and additionally allowed regions, further supporting the structural accuracy of the predicted model. The query sequence (Uniprot ID Q14439) with Isoform ID: Q14439-1 can be found in the supplementary file.

Model validation

The validation of the modeled 3D structure for the GPR176 protein was performed using DeepTMHMM (https://dtu.biolib.com/DeepTMHMM). This was done to predict the seven transmembrane helices and match the helical regions in the AlphaFold model, supporting the reliability of the modeled protein.

Binding site analysis

To identify the potential binding sites required for downstream docking simulations, binding site prediction was performed using the SiteMap tool integrated within Maestro (Schrödinger Suite version 13.5). The modelled GPR176 structure was first imported into Maestro, and its visualization was optimized using the "Preset" function. The protein structure was then refined using the Protein Preparation Wizard, which added missing hydrogen atoms, assigned bond orders, optimized hydrogen bonding networks, and removed water molecules. Following preparation, the SiteMap tool was utilized to analyze the 3D structure for possible ligand-binding pockets. SiteMap uses spatial, topological, and physicochemical features such as hydrophobicity, hydrogen bonding capacity, and site size to rank binding sites (Alzyoud et al., 2022). The active site with the highest SiteScore and DScore was selected for molecular docking. Subsequently, a Receptor Grid was generated around the predicted binding pocket using the Receptor Grid Generation module in Maestro. This grid defines the docking space and ensures that ligands are evaluated specifically within the active site during docking simulations (Hasan, 2025).

Molecular docking

Preparation of ligands

A library of 372 compounds was obtained from ReDO_DB (the Repurposing Drugs in Oncology database), an open-access database of natural products derived from approved compounds exhibiting anticancer activity (http://www.redo-project.org/db/)[25]. The compounds were downloaded in SDF format and imported into Maestro 13.5 (the unified graphical interface of Schrödinger Suite) for processing[35]. The ligand structures and vismodegib structure (control) were optimized using the LigPrep tool, where ionization states were generated at physiological pH (7.0 ± 2.0) by the Epik module, and energy minimization was performed under the OPLS4 force field, and stereoisomers were retained[35]. The prepared ligands were subsequently used for docking.

Target protein preparation

The modeled three-dimensional structure of the G protein-coupled receptor (GPR176) was prepared using the Protein Preparation Wizard in Maestro, which involved assigning bond orders, adding missing side chains, addressing overlapping hydrogens, optimizing hydrogen bonding networks, performing energy minimization, and removing water molecules from the protein[3637]:.

Receptor grid generation

The active site of GPR176 was defined using the Sitemap tool in the Maestro glide application (Bender et al., 2021). Grid generation was carried out using the Receptor Grid Generation tool in Glide, ensuring that the box dimensions encompassed the binding pocket and allowed adequate ligand flexibility[33,38]. The receptor grid box resolution was centered at coordinates 159.97, 168.47, and 194.06, corresponding to the x, y, and z-axis, respectively.

Docking simulation

Molecular docking using the Schrodinger Maestro Suite version 13.5[35,38]. Prepared ligands were subjected to molecular docking using Glide docking methodology (Schrödinger) in extra precision (XP) mode, also known as Grid-based Ligand Docking with Energetics (Glide XP)[38]. Glide XP was used because of its remarkable precision[38]. The docking algorithm evaluated ligand poses within the defined active site, and the best conformations were scored using the docking score and the GlideScore[35,38]. The top-ranked ligands, together with the control, were further subjected to induced fit docking using Maestro 13.5.

Protein–ligand interaction analysis

Top-ranking protein–ligand complexes were analyzed using the Ligand Interaction Diagram tool in Maestro to visualize key interactions such as hydrogen bonds, hydrophobic contacts, and π–π stacking with active site residues[36]. Binding affinity was assessed based on docking score and GlideScore, and only ligands with significant docking scores were selected for further analysis[35,38].

Free energy rescoring using prime-MMGBSA

Molecular Mechanics/General Born Surface Area (MM-GBSA) analysis was performed to more accurately evaluate the binding free energies of ligands bound to the GPR176 protein, whose 3D structure was predicted by homology modeling (Genheden S, 2015). This analysis was performed using the Prime MM-GBSA module in Schrödinger Maestro 14.3. Protein-ligand complexes that obtained scores after molecular docking were re-evaluated with the MM-GBSA protocol.

This method takes into account molecular mechanics energies (MME), solvent effects (polar and apolar), and conformational contributions to calculate the binding energy (ΔG_{bind}) employing the expression: $E_{(minimized\ complex)} = E_{(minimized\ protein)} - E_{(minimized\ ligand)}$. Thus, a more accurate binding energy estimate was provided beyond the docking scores (Tuccinardi, 2021).

Density functional theory quantum calculations (DFT)

The molecular geometries of all selected ligands (Table 1) were optimized employing the B3LYP hybrid functional[32] within the Gaussian 16 computational package[39]. For this purpose, the 6–31G(d, p) basis set was applied to every atom. The optimized structures obtained from these calculations were subsequently utilized as the starting conformations for docking and molecular dynamics studies. At the same theoretical level, electronic characteristics such as Mulliken charge distribution and the HOMO–LUMO energy gap were also evaluated to provide insight into the electronic framework of the ligands. Furthermore, global reactivity descriptors were derived via Fukui function analysis to evaluate the compound's chemical reactivity[40].

Molecular dynamics simulations

Molecular dynamics (MD) simulations were conducted for the two most effective ligands (Fostamatinib and Ticagrelor) from the docking studies and the control compound Vismodegib against the GPR176 protein. All systems, comprising the apo protein and protein-ligand complexes, were prepared using the CHARMM-GUI web server[41]. Each system was solvated in a cubic box of TIP3P water[42], maintaining a minimum distance of 10 Å between the solute and the box edge. Ionic strength was set to 0.15 M using potassium and chloride ions. The CHARMM36 all-atom force field[43] was applied to the protein, while ligands were parameterized with the CGenFF force field[44]. An energy minimization of 1000 steps was first performed using the Adopted Basis Newton-Raphson algorithm. Systems were then equilibrated with a 1 ns simulation in the NVT ensemble, followed by a 5 ns simulation in the NPT ensemble. Subsequently, production MD runs were carried out for 100 ns using GROMACS 2022[45] at a constant pressure of 1 atm and a temperature of 300 K. Long-range electrostatic

Name of the compounds used as ligands	2D structures
Fostamatinib	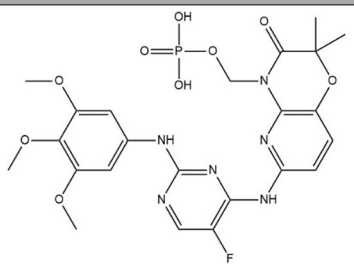
Ticagrelor	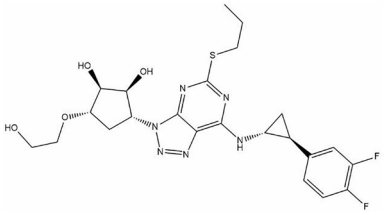
Vismodegib (control)	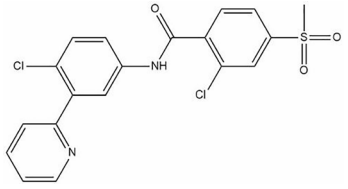

Table 1. Structure of the selected ligands.

interactions were treated with the Particle Mesh Ewald (PME) method[46,47], and a 12 Å cutoff was applied for short-range van der Waals and Coulomb interactions. An integration timestep of 1.0 fs was used, and trajectories were saved every 20 ps for analysis.

Absorption, distribution, metabolism, and excretion (ADME)

The pharmacokinetic profile of the selected ligands, Fostamatinib and Ticagrelor, was evaluated in silico by predicting their Absorption, Distribution, Metabolism, and Excretion (ADME) parameters using the SwissADME online tool[48]. For this analysis, the canonical SMILES representation of those ligands was employed as the initial input, from which a detailed profile of molecular descriptors was generated. Key evaluated metrics included fundamental physicochemical properties such as molecular weight, number of rotatable bonds, and hydrogen bond donor and acceptor counts. The assessment also covered lipophilicity (Log P o/w), solubility (Log S), and key pharmacokinetic parameters like gastrointestinal absorption, blood-brain barrier permeation, and CYP450 enzyme inhibition potential[48]. These computational ADME predictions offer essential preliminary data on the compound's bioavailability and pharmacokinetic behavior to guide subsequent experimental validation.

Toxicology profile prediction

The toxicology profile of the Fostamatinib and Ticagrelor was obtained by implementing the ProTox-3.0 server[49]. The evaluated parameters were Organ toxicity, Toxicity endpoints, Nuclear receptor signalling pathways, Molecular Initiating Events, and Metabolism[50].

Results

Homology modelling

The three-dimensional structure of GPR176 (305 amino acids) was successfully generated through homology modeling and evaluated for structural reliability. The resulting protein model had a 100% identity and sequence coverage of 1 with the template (human GRP176: Q14439.1.A) obtained from Alphafold DB.

The overall quality check performed with ProSA-web yielded a Z-score of −1.79 (Fig. 2), which is within the range commonly reported for correctly folded GPCR models[51]. As visualized in the ProSA model quality plot, the black dot representing the GPR176 model lies well within the dense clusters of known X-ray and NMR-resolved structures. This suggests that the model has acceptable structural quality and is suitable for downstream computational studies. This suggests that the generated model falls within acceptable limits and is suitable for downstream computational studies such as docking and molecular dynamics[52,53].

Further stereochemical evaluation with PROCHECK showed that 93.0% of residues were located in the most favored regions of the Ramachandran plot, 6.6% were in additionally allowed regions, and only 0.3% (1 residue) was positioned in a disallowed region (Fig. 3). These results indicate that the GPR176 model demonstrates a high level of stereochemical accuracy. Recent evaluations emphasize that homology models with > 90% residues in favored regions are generally considered structurally reliable and are widely used in GPCR docking and simulation workflows[51,54].

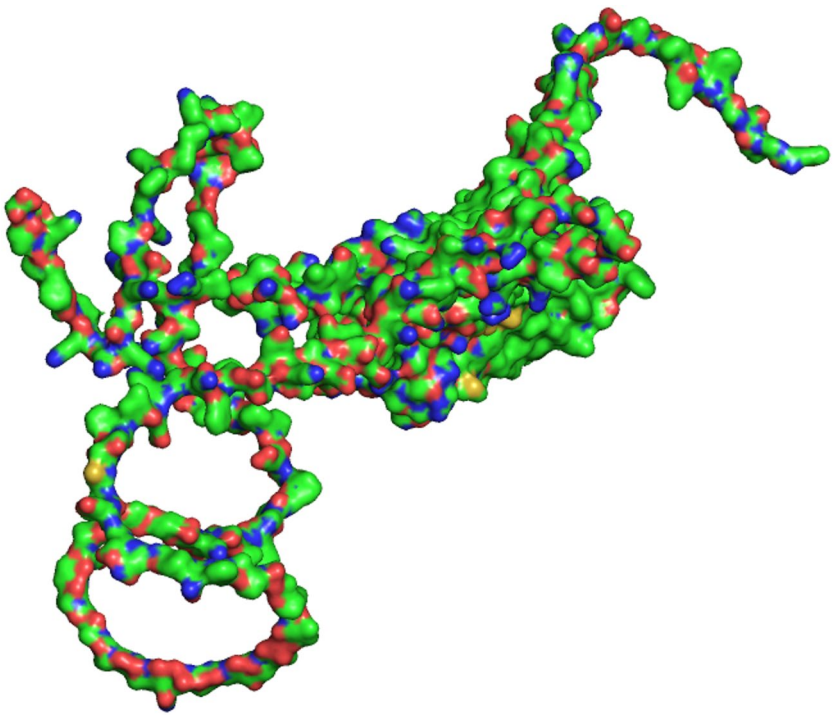

Fig. 2. Overall quality assessment of the GPR176 homology model using ProSA-web Z-score.

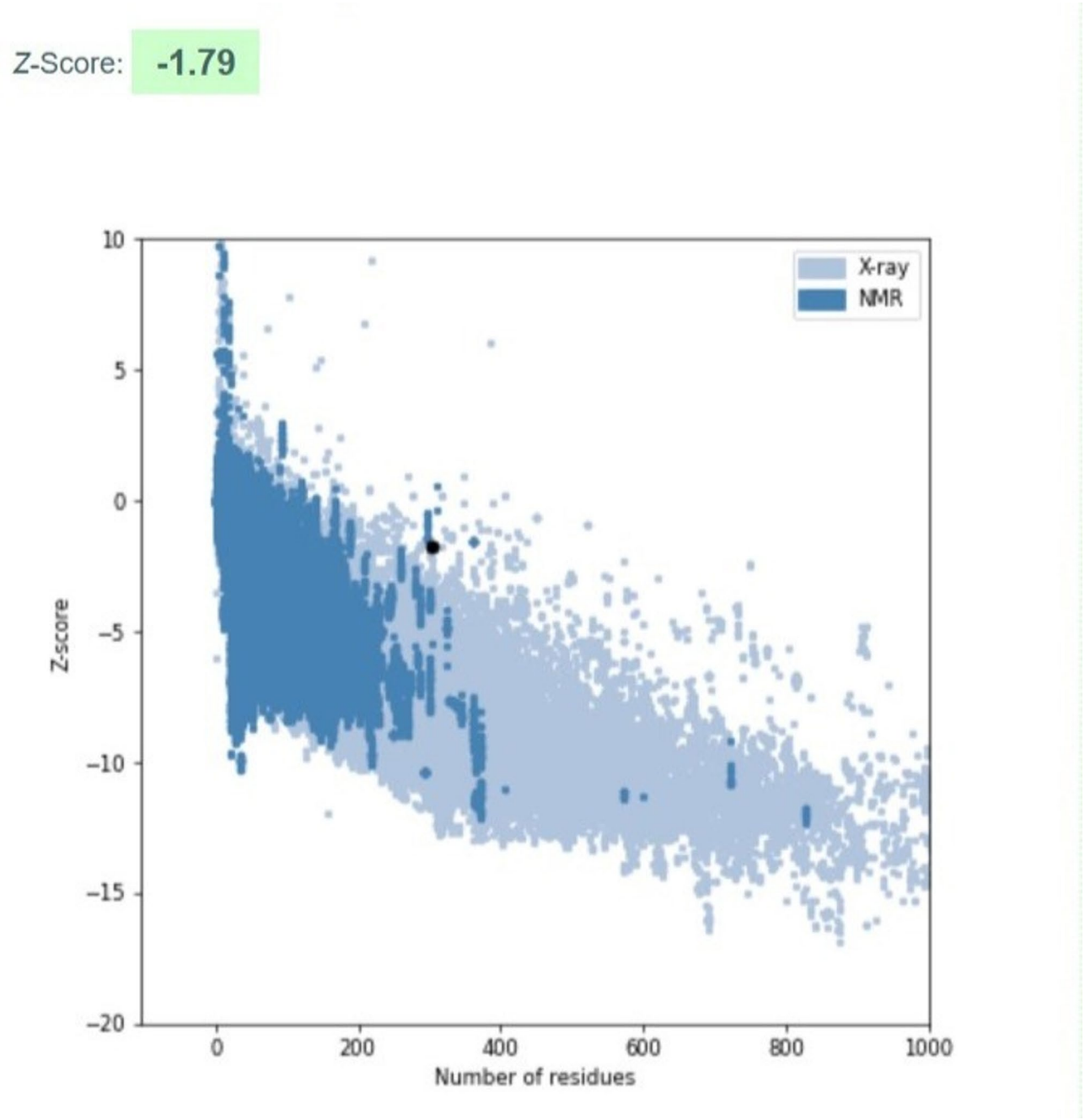

Fig. 3. Ramachandran plot validation of the GPR176 homology model generated by procheck.

Validation from DeepTMHMM

The validation protocol from the DeepTMHMM corroborated the structural integrity of the modelled GPR176 protein from AlphaFold. The DeepTMHMM server predicted seven well-defined transmembrane helices (43–64, 79–102, 119–140, 162–180, 206–226, 268–291, 301–321), which are in alignment with the helical bundle in the modelled 3D structure (supplementary files). These segments also align with the regions of highest pLDDT, whereas lower-confidence values are restricted to loop and terminal regions, which are expected to be flexible in GPCRs. This agreement between two independent deep-learning methods strengthens the reliability of the modeled transmembrane core used in downstream docking analyses.

Molecular docking

The results from the docking simulations of the compounds retrieved from the ReDO_DB and the modelled GPR176 are shown in Table 2. Out of the 372 ligands and control docked to GPR176, nine (9) were found to have docking scores between −8.449 kcal/mol and −7.513 kcal/mol, which is higher than the docking score of the control (vismodegib) −2.361 kcal/mol. The induced fit docking (IFD) of the nine compounds ranges

Name	Docking score kcal/mol	IFD	Docking Score after IFD (kcal/mol)
Fostamatinib	−8.449	−577.77	−11.503
Ticagrelor	−7.513	−573.06	−11.882
Vismodegib	−2.361	−568.91	−10.759
Cidofovir	−7.513	−563.6	−7.42
Risedronic acid	−8.326	−562.35	−9.995
Ibandronic acid	−7.916	−561.64	−8.083
Alendronic acid	−7.998	−559.51	−7.126
Zoledronic acid	−8.213	−559.44	−8.029
Clodronic acid	−7.580	−558.85	−9.666
Pamidronic acid	−8.131	−557.3	−7.69

Table 2. The docking scores of the top 9 compounds.

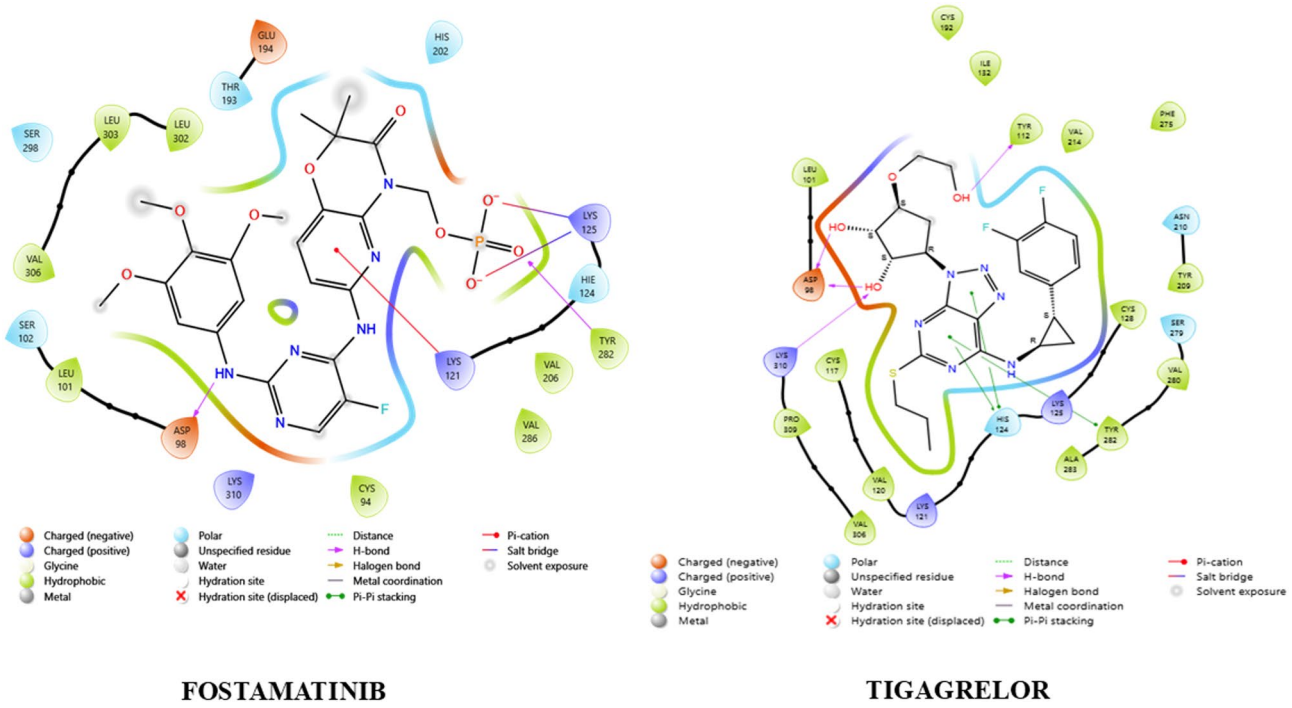

Fig. 5. 2D interactions of Fostamatinib and Ticagrelor at the binding site.

from −577.77 to 559.44. It revealed that only two drug compounds, Fostamatinib (−577.77) and Ticagrelor (−573.06), performed better than Vismodegib with an IFD score of −568.91; the redocking after IFD affirms the binding strength of Fostamatinib and Ticagrelor to the GPR176 protein with docking scores of −11.503 kcal/mol and −11.882 kcal/mol, respectively, compared to Vismodegib (−10.759 kcal/mol). These findings suggest that Fostamatinib and Ticagrelor have the highest binding affinity for G protein-coupled receptor 176 (GPR176) among the control drug (vismodegib) and could serve as hit compounds for the discovery of GPR176 inhibitors.

These drug compounds had interactions with the amino acid residue at the binding crevice. Fostamatinib had diverse reactions with the residues at the binding pocket of the GPR176 protein (Fig. 5). It formed positively charged bonds with Lys 121, 125, and 310; Negatively charged interactions with Asp 98 and Glu 194; Polar bonds with Ser 102 and 298, Thr 193, and His 202. It reacted via hydrophobic bonding formations with residues Cys 94, Leu 101, Val 206, Tyr 282, Val 286, Leu 302 and 303, and Val 306 (Fig. 4). Tigagrelol was meshed at the binding pocket of GPR176 (Fig. 5). The drug molecule reacted with the protein via largely hydrophobic interactions by forming bonds with Leu 101, Cys 117, Val 120, Pro 309, Val 306, Ala 283, Tyr 282, Val 283, Cys 128, Tyr 209, Val 214, Phe 275, Tyr 112, Ile 132, Cys 192; Postively charged interactions with Lys 121, 125, and 310 and finally a negatively charged interactions with Asp 98 (Fig. 6).

Molecular mechanics, generalized born surface area (MMGBSA)

The MMGBSA was employed to predict the binding free energy between the compounds and the protein[55]. These results (Table 3) corroborate the findings from the docking simulations. Ticagrelor had the highest binding free energy of −93.86 kcal/mol, which indicates that it docked in the binding pocket with high affinity

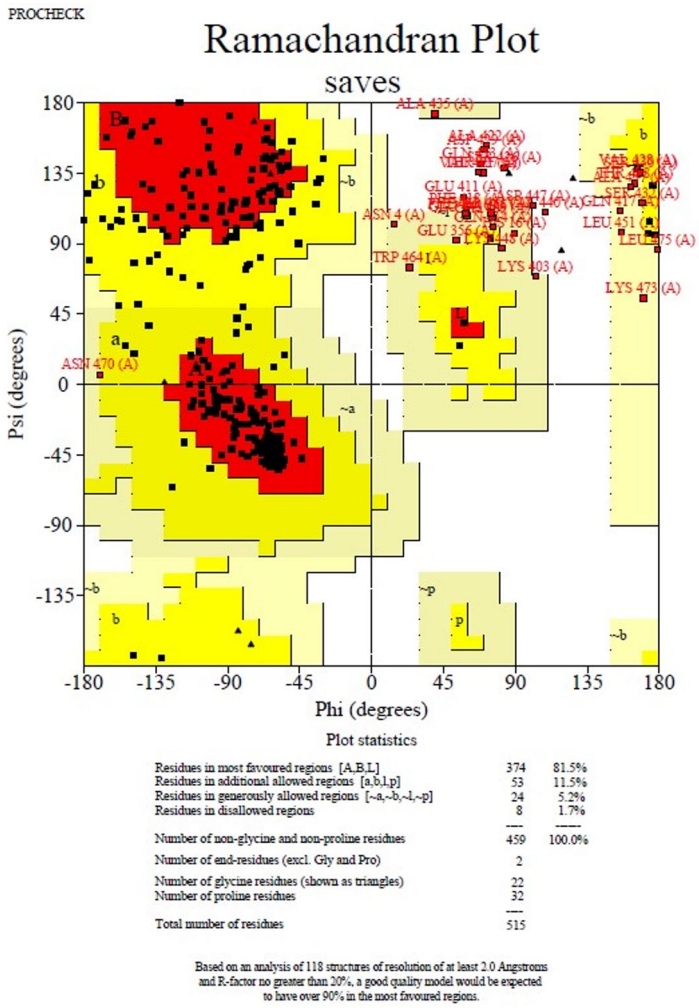

Fig. 4. 3D interaction of Fostamatinib with GPR176.

and could significantly affect the conformational stability of the protein. Fostamatinib, bound with an energy of −72.54 kcal/mol, reached a value close to Vismodegib but maintained its advantageous position in terms of stability. The binding free energy (ΔG binding) was significant for both drug molecules and showed lower values compared to the control molecule. Overall, Ticagrelor and Fostamatinib appear to have the potential to modulate the protein's functional domains by forming multiple hydrogen bonds and hydrophobic interactions in the binding site (Table 3).

DFT-based analysis

Figure 7 represents the optimized structures of the ligands used for the molecular dynamics study.

Mulliken charge distribution

The Mulliken charge distribution (Fig. 8) illustrates that Fostamatinib and Ticagrelor display marked polarization concentrated around their heteroatoms, whereas Vismodegib shows a comparatively uniform pattern. In both Fostamatinib and Ticagrelor, electronegative atoms, such as phosphate or carbonyl oxygens and triazole/adenine nitrogens, bear substantial negative charges, with adjacent hydrogen-linked carbons carrying compensatory positive charges. This uneven charge allocation highlights potential reactive regions—negatively charged sites likely serving as hydrogen-bond acceptors and positively polarized sites as probable electrophilic centers. In contrast, Vismodegib exhibits milder charge separation across its framework, consistent with its predominantly aromatic scaffold and reduced polarity. Overall, the stronger charge localization and higher dipole tendencies of Fostamatinib and Ticagrelor suggest the presence of more distinct and accessible reactive sites compared with the control compound.

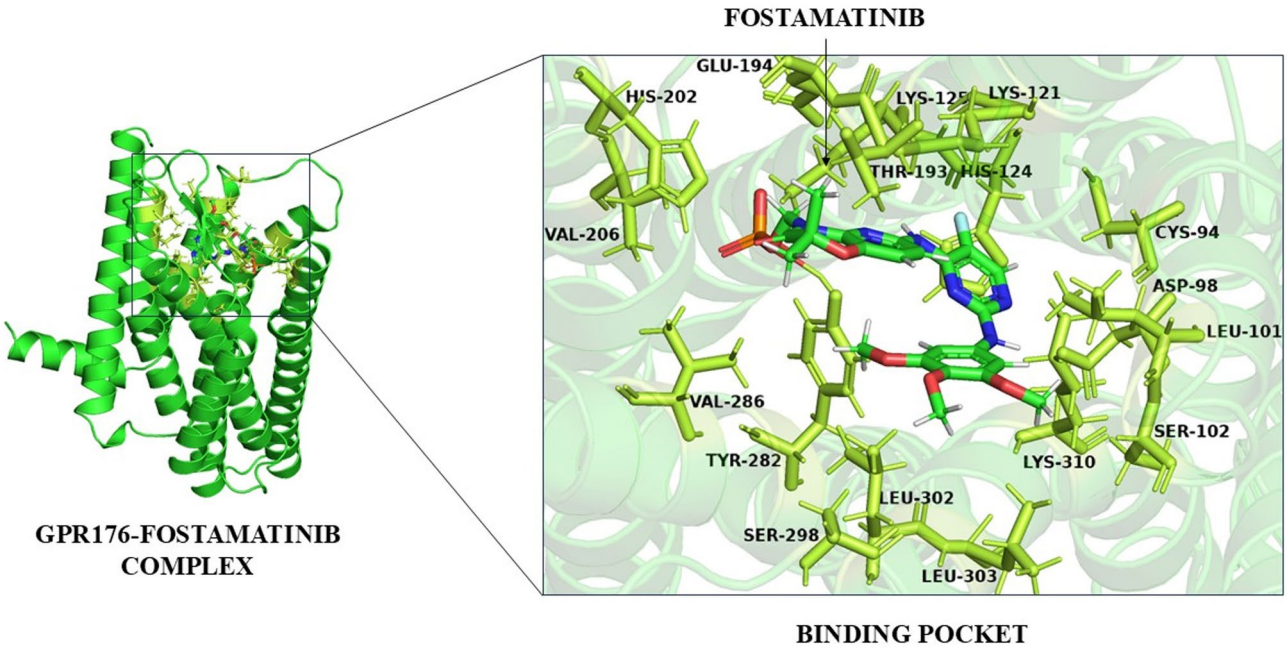

Fig. 6. 3D interactions of Ticagrelor with GPR176.

Name	MMGBSA (Kcal/mol)
Fostamatinib	−72.54
Ticagrelor	−93.86
Vismodegib	−73.04
Cidofovir	−43.47
Risedronic acid	−13.40
Ibandronic acid	−37.80
Alendronic acid	−12.39
Zoledronic acid	−28.50
Cloronic acid	−10.63
Pamidronic acid	−1.39

Table 3. MMGBSA scores for the drug molecules.

HOMO–LUMO gap and reactivity
DFT results indicate that Vismodegib exhibits the widest HOMO–LUMO energy separation (Fig. 8), while the tested drug molecules, Fostamatinib and Ticagrelor, display comparatively narrower gaps. The energy gaps for the Fostamatinib and Ticagrelor were 5.79 eV and 5.32 eV, respectively, while Vismodegib was 6.47 eV.

Global reactivity parametersGlobal reactivity parameters
The global reactivity indices (Table 4) further support these observations. The chemical hardness for Fostamatinib and Ticagrelor were 0.2128 and 0.1958, respectively, while vismodegib had the highest of 0.2378. Fostamatinib and Ticagrelor possess narrower HOMO–LUMO gaps; they show reduced global hardness (η) and correspondingly increased global softness (S = 1/η) of 4.6986 and 5.108, respectively, relative to Vismodegib (4.2049). For the chemical potential, Fostamatinib scored 0.1327, Ticagrelor had −0.1296, while Vismodegib scored −0.1371 (Table 4).

Molecular dynamics analysis of GPR176-ligand complexes

RMSD (Root Mean Square Deviation): RMSD measures the average deviation of protein atomic positions over time, with lower RMSD indicating higher structural stability. In RMSD plots (Fig. 9), the Fostamatinib-bound complex equilibrates to a lower RMSD (~0.30–0.40 nm) than the unliganded protein (~0.40–0.50 nm), indicating that Fostamatinib stabilizes the protein structure. In contrast, the Ticagrelor complex shows larger deviations, rising to ~0.50 nm by 50–60 ns, suggesting greater conformational fluctuation. Vismodegib (control) lowers the RMSD modestly (~0.30–0.40 nm vs. ~0.45 nm apo), similar to Fostamatinib. Quantitatively, the time-averaged RMSD of GPR176 + Fostamatinib (~0.35 nm) is smaller than that of Ticagrelor (~0.45 nm),

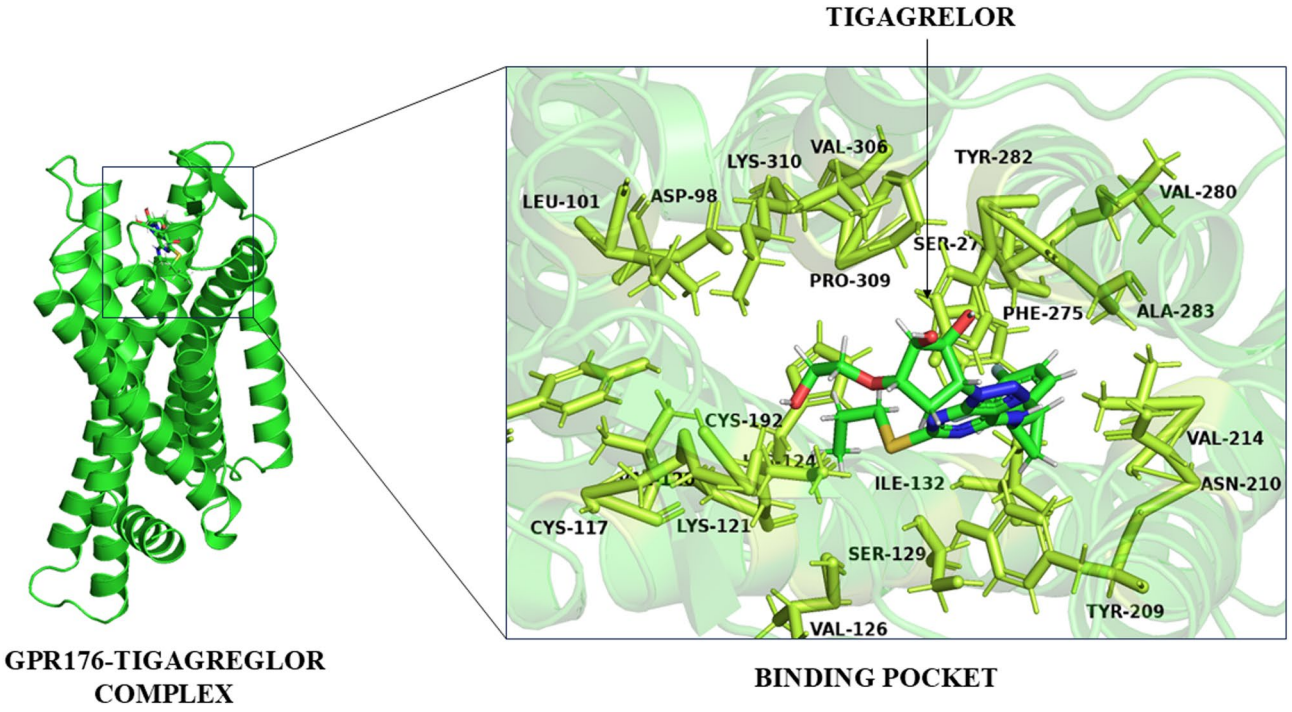

Fig. 7. Optimized structure of the selected ligands.

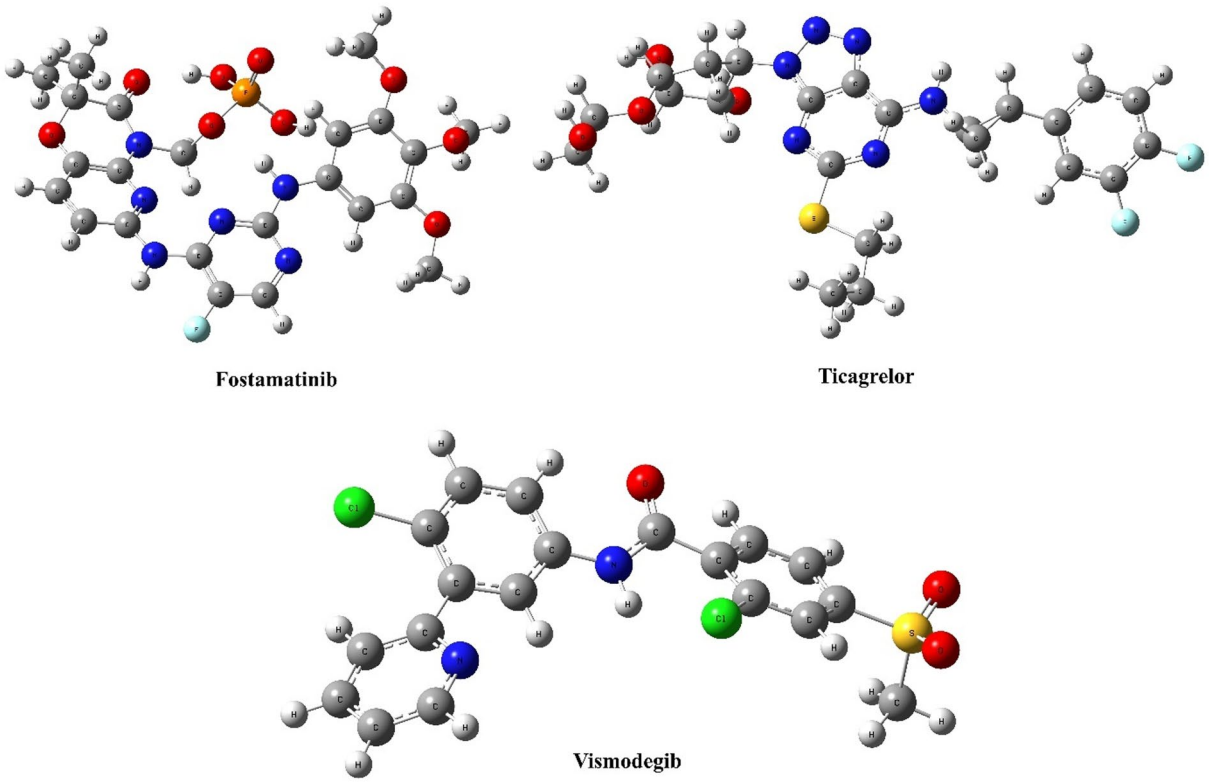

Fig. 8. Mulliken charge analysis and HOMO-LUMO gap measurement of the selected ligands.

Name of the compound	Global reactivity parameters			
	Electronic potential (au)	Global hardness(au)	Global softness(au)	Electrophilicity (eV)
Fostamatinib	−0.1327	0.2128	4.6986	1.1256
Ticagrelor	−0.1296	0.1958	5.108	1.167
Vismodegib (control)	−0.1371	0.2378	4.2049	1.0757

Table 4. Global reactivity parameters.

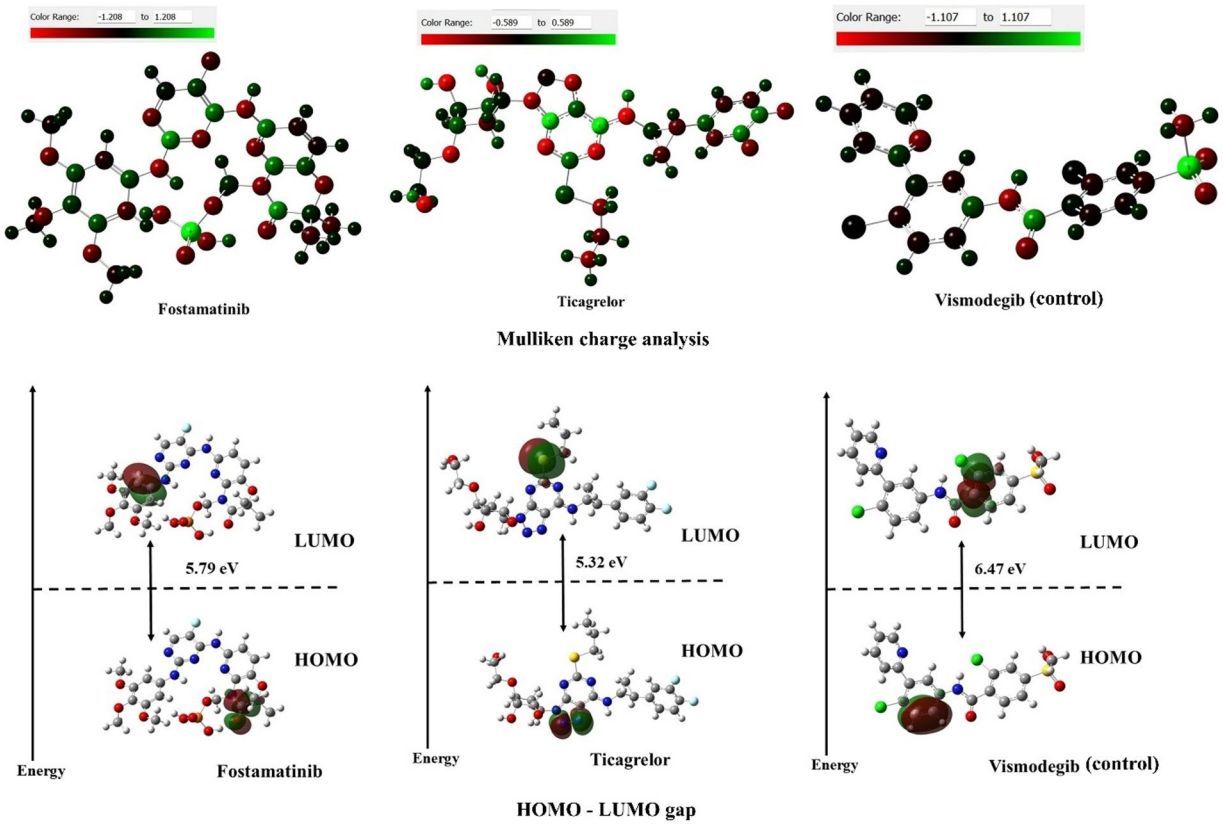

Fig. 9. RMSD plots for GPR176 with different ligands.

implying that Fostamatinib binding yields the most rigid complex (lower RMSD) among the test ligands. These trends are consistent with the idea that sustained low RMSD reflects a more stable ligand-bound structure.

Radius of gyration (Rg)RMSF (root mean square fluctuation)

RMSF (Root Mean Square Fluctuation): RMSF quantifies per-residue flexibility (mean deviation from the average structure) during the simulation. In all cases of RMSF profiles (Fig. 10), loops and termini exhibit the highest fluctuations. Binding Fostamatinib reduces many peak fluctuations: for example, residues ~ 250–300 have RMSF peaks ~ 0.60–0.65 nm in the apo protein but only ~ 0.50 nm when Fostamatinib is bound. This indicates that Fostamatinib dampens motions in flexible regions. By contrast, Ticagrelor causes some regions to fluctuate more (e.g., residue ~ 250 has ~ 0.75–0.80 nm vs. ~ 0.65 nm apo), meaning it does not stabilize those loops as effectively. Vismodegib produces intermediate effects: it mildly lowers peaks near residue 250 (to ~ 0.55–0.60 nm) and near residue 300 (~ 0.65 vs. ~ 0.70 nm apo). Overall, Fostamatinib yields the greatest reduction in RMSF, reflecting enhanced rigidity; Ticagrelor's profile shows higher peaks, reflecting less restrained dynamics.

Radius of gyration (Rg)

Rg measures the overall compactness of the protein (mass-weighted spread of atoms around the center of mass). Radius of gyration (Rg) of GPR176 in different complexes is represented by (Fig. 11). All complexes fluctuate narrowly around ~ 2.20–2.25 nm, indicating no large unfolding. The Fostamatinib complex consistently has a slightly lower Rg (~ 2.18–2.22 nm) than the apo protein (~ 2.22–2.25 nm), implying a modest compaction. Ticagrelor shows Rg essentially overlapping apo (~ 2.20–2.25 nm) with no clear reduction in size. The Rg profile of the Vismodegib complex (black) remains in the range of ~ 2.20–2.24 nm. In comparison, Fostamatinib binding results in a slightly lower Rg value, indicating a modest compaction of GPR176 relative to both Ticagrelor and

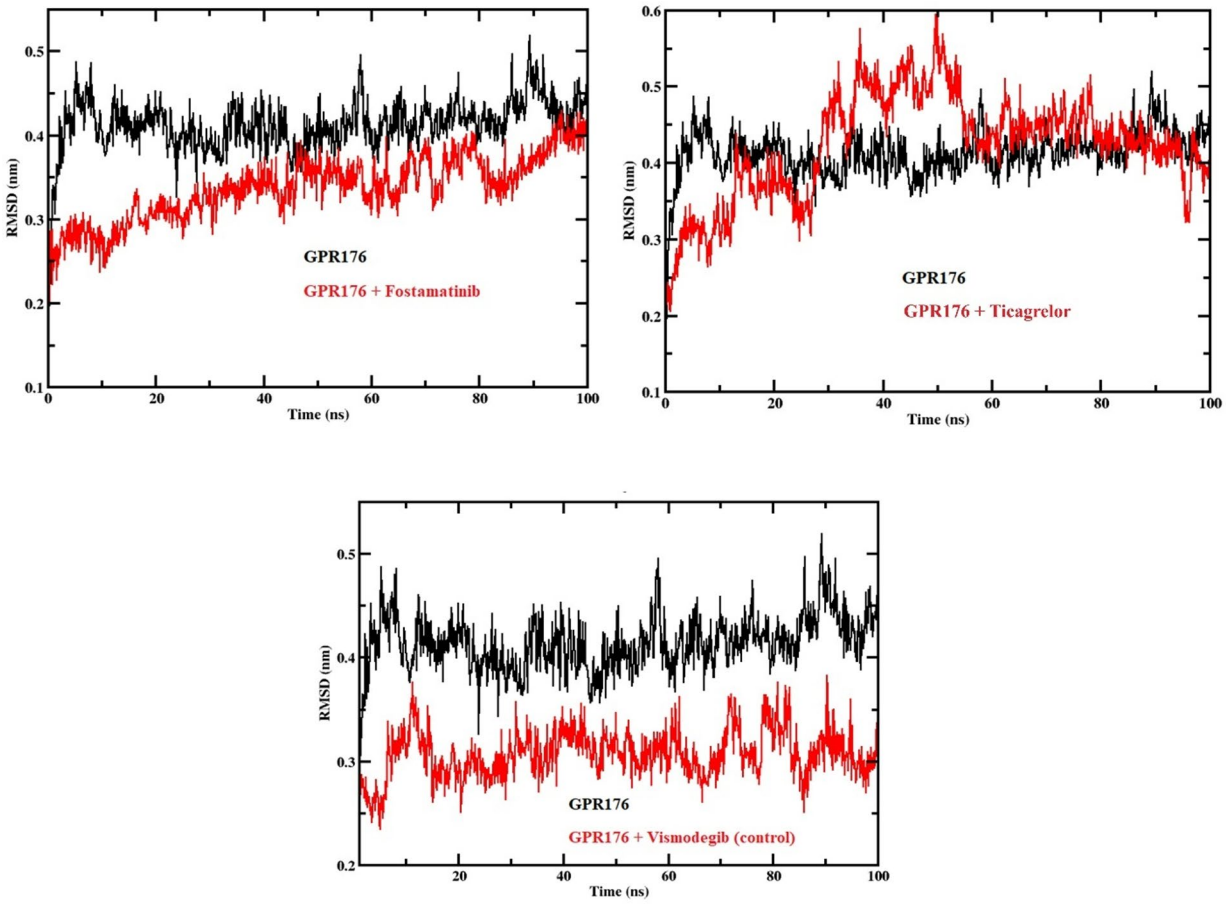

Fig. 10. RMSF plots for GPR176 with different ligands.

the control. Despite this difference, all ligand–protein systems display overall globular conformations without evidence of large-scale unfolding. The subtle decrease in Rg observed with Fostamatinib supports its role in promoting structural stabilization of the receptor.

Ligand–receptor distance

The distance between ligand and protein (e.g., ligand center-of-mass to binding site) reflects binding position and stability, as reflected by Fig. 12. All three remain relatively constant after ~ 10–20 ns, indicating stable binding. Ticagrelor maintains the shortest distance (~ 1.3–1.6 nm), but has more fluctuation in the binding pocket. Vismodegib fluctuates around ~ 1.6–1.7 nm. Fostamatinib shows a larger mean distance (~ 2.0–2.2 nm) with less fluctuation, maintaining a constant distance. These values imply that Fostamatinib binds with a somewhat more extended orientation (perhaps interacting with different protein regions. Despite this, all trajectories plateau quickly, meaning none of the ligands dissociates; the constant distances imply continued binding throughout the 100 ns.

Hydrophobic contacts and hydrogen bonds

Non-covalent interactions between ligand and receptor were quantified by contact counts (Fig. 13). Number of hydrophobic contacts (top) and hydrogen bonds (bottom) over time for each ligand–GPR176 complex. Ticagrelor has the highest hydrophobic contact count, rising to ~ 50–60 contacts and staying high, whereas Fostamatinib (red) peaks ~ 30–40 contacts and Vismodegib (black) ~ 20–25. In contrast, Fostamatinib forms the most H-bonds (~ 2–5 simultaneously), while Ticagrelor rarely exceeds 1–2, and Vismodegib rarely forms any. Thus, Fostamatinib relies heavily on polar interactions (many H-bonds) to bind, whereas Ticagrelor is stabilized by hydrophobic packing. Vismodegib makes relatively few of both, as expected for a control. As noted in the literature, both hydrogen bonding and hydrophobic interactions contribute to ligand stability. The interaction pattern of Fostamatinib, characterized by stable hydrogen bonds together with a moderate number of hydrophobic contacts, indicates a strong and well-defined binding mode. In contrast, Ticagrelor exhibits a predominance of hydrophobic contacts, reflecting a close nonpolar association, although its limited hydrogen bonding suggests reduced binding specificity. Vismodegib demonstrates an intermediate profile, aligning with its function as a comparative reference ligand in this study.

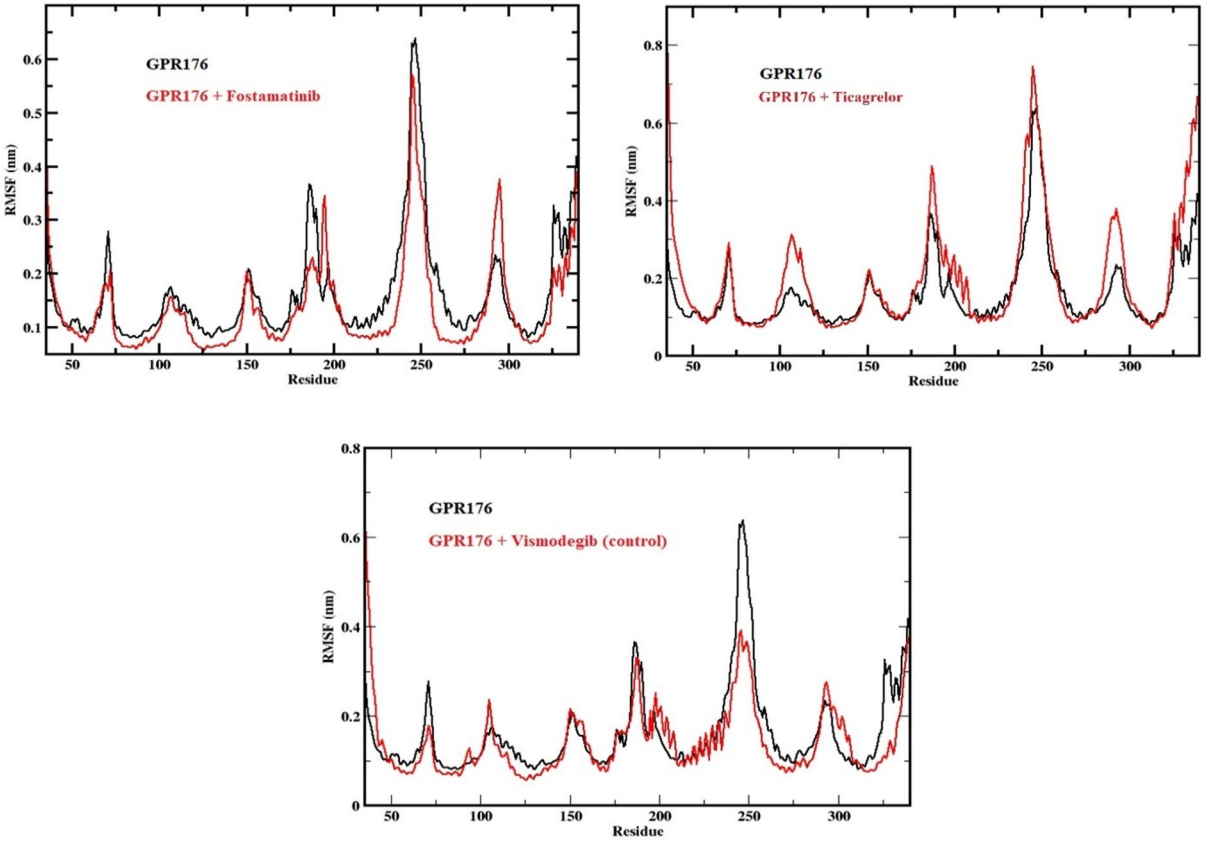

Fig. 11. Radius of Gyration plot for GPR176 with different ligands.

ADMET profile comparison of fostamatinib and Ticagrelor
The pharmacokinetic features of limonene were examined (Table 3) using the SWISS ADME platform to evaluate its suitability as a lead-like compound.

Physicochemical properties
Fostamatinib (molecular weight ≈ 580 Da) is notably larger and more polar compared with Ticagrelor (molecular weight ≈ 522 Da). While both ligands possess three aromatic rings, Fostamatinib has a greater number of heavy atoms (40 versus 36) and demonstrates a substantially larger topological polar surface area (PSA ≈ 186.7 $Å^2$ versus 138.4 $Å^2$). Correspondingly, fostamatinib has many polar functionalities (12–13 H-bond acceptors and 4 H-bond donors) while Ticagrelor has slightly fewer acceptors (11) with the same number of donors (4). Both molecules have a high number of rotatable bonds (10 each), reflecting flexibility. Fostamatinib's relatively low fraction of sp^3 carbons (0.30) vs. Ticagrelor's (0.57) suggests that Ticagrelor is more saturated (more sp^3 centers) while Fostamatinib is more aromatic.

Lipophilicity
Multiple computed log P values indicate that Ticagrelor is more lipophilic than fostamatinib. For example, Chemistry Development Kit (CDK) predictions give XLogP ≈ 1.06 for fostamatinib versus ≈ 2.01 for Ticagrelor. Consensus log P predictions (averaging methods like iLOGP, XLOGP3, etc.) similarly show Ticagrelor around ~ 2.4 vs. fostamatinib ~ 1.7 (SwissADME consensus) – a clear difference consistent with Ticagrelor's higher nonpolar character. Thus, Ticagrelor is expected to partition more into lipid phases than fostamatinib, which is relatively polar (low log P).

Water solubility
Both compounds have very limited aqueous solubility. Fostamatinib's water solubility is on the order of 0.05 mg/mL (predicted by ALOGPS), classifying it as poorly to moderately soluble. Ticagrelor's solubility is even lower (≈ 0.01 mg/mL) – indeed, it has been noted to exhibit *"low solubility"* in water. Thus, neither drug is highly soluble; computational models (ESOL, Ali) may label them "moderately soluble", but the absolute values are quite low. In fact, one solubility predictor (SILICOS-IT) flags fostamatinib as poorly soluble (log S ~–6.1), whereas Ticagrelor remains moderately soluble (log S ~–4.9), reflecting that Ticagrelor is modestly easier to dissolve despite being lipophilic. Overall, poor aqueous solubility is a challenge for both molecules, more so for fostamatinib, which is predicted to be at the edge of "poor" solubility.

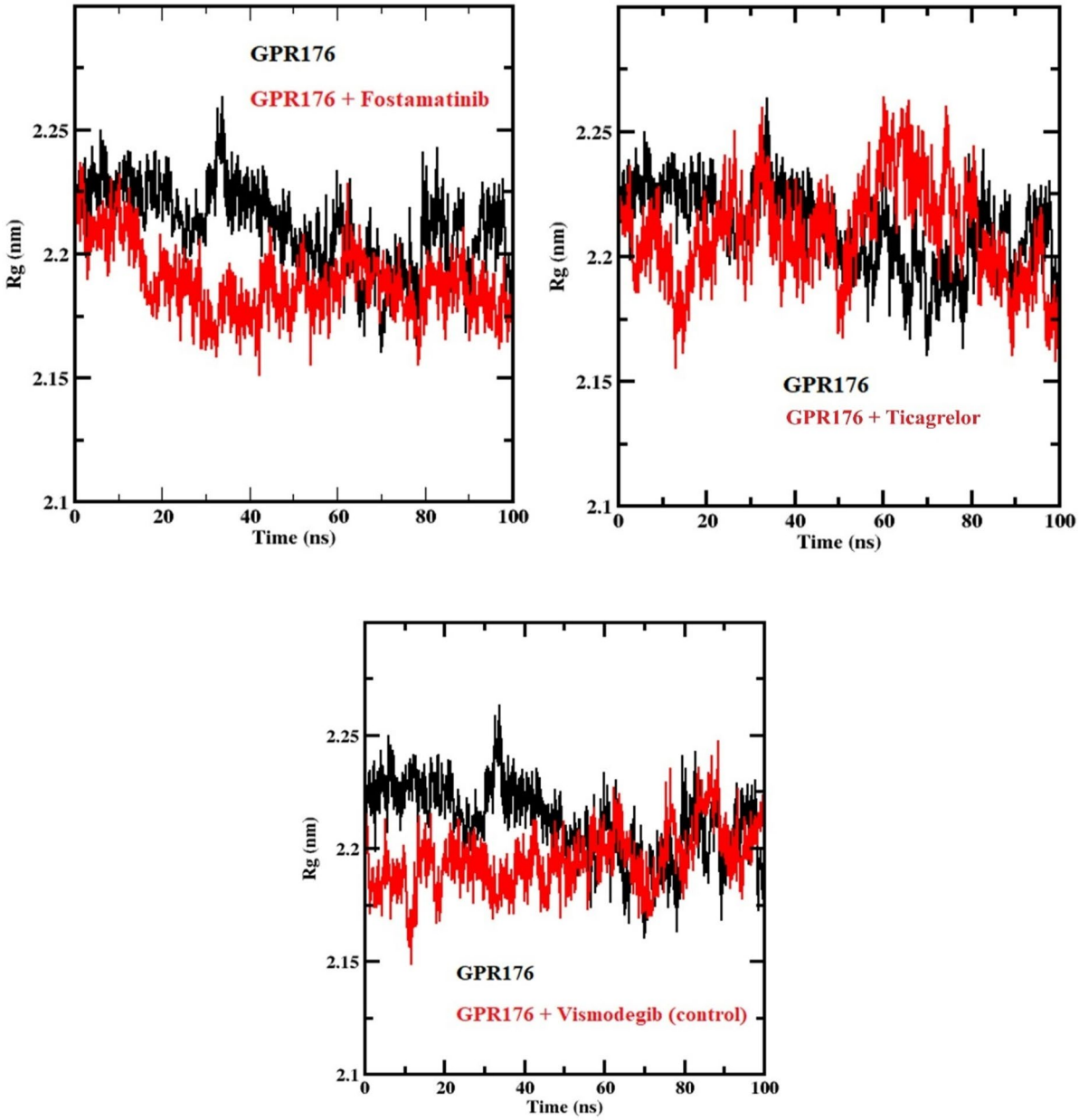

Fig. 12. Distance plot showing hydrophobic interactions between the GPR176 protein and different ligands.

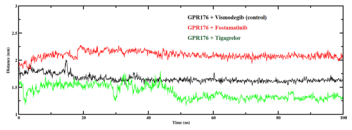

Fig. 13. Hydrophobic contacts and Hydrogen bonding between the GPR176 protein and different ligands.

Pharmacokinetics

Both drugs are predicted to have *low gastrointestinal (GI) absorption*, largely due to their high polarity and large size. Neither compound readily crosses the blood–brain barrier (non-BBB permeant), given their high PSA and H-bond counts (well above typical BBB thresholds). Both are predicted substrates of P-glycoprotein efflux (P-gp substrate: yes for both). For instance, fostamatinib's active metabolite R406 is documented as a P-gp substrate and also inhibits P-gp in vitro, and Ticagrelor has been reported to interact with P-gp (inhibiting it). Neither drug is expected to inhibit most CYP enzymes (CYP1A2, 2C19, 2C9, 2D6 inhibitors: all 'No'). Notably,

both compounds do inhibit CYP3A4: fostamatinib's metabolite R406 is a CYP3A4 inhibitor, and Ticagrelor is known to be a (weak) CYP3A4 inhibitor. Skin permeation (log Kp) is extremely low for both (around − 8 cm/s), implying negligible transdermal absorption (consistent with high polarity).

Toxicology profile

The ProTox-3.0 was employed to compare the toxicology profiles of top-performing compounds. The LD50 Values for Fostamatinib were 2935 mg/kg, placing it in toxicity Class V; Ticagrelor had a value of 29 mg/kg, placed in toxicity Class II, while the control, Vismodegib, is predicted to be in Class V; its LD50 value was 5000 mg/kg.

For their organ toxicity tendencies, all three compounds revealed no cardiotoxic tendencies. Fostamatinib and Ticagrelor were revealed to have a high probability for respiratory toxicity. Fostamatinib had a probability of 0.86, and Ticagrelor had 0.95, while Visomdegib had 0.86. None of the three compounds was indicated to be carcinogenic or cytotoxic. They were revealed to be potentially active with the Blood Brain Barrier, with the control having a higher probability (0.87) of being toxic to the tissue (Table 6).

In their toxicity in the nuclear receptor signalling pathways and their initiating activity for molecular events, fortunately, none of the three compounds were revealed to be potentially active with the receptors, enzymes, and factors examined, with the lowest probability from the control (0.53) in their character to activate the Thyroid hormone receptor beta (THRβ) and the Pregnane X receptor (PXR). In the same instance, the compound had a strong tendency not to hamper the safety of the alpha-amino-3-hydroxy-5-methyl-4-isoxazolepropionate receptor (AMPAR) and Kainate receptor (KAR) associated molecular events. Vismodegib had a probability of 1, while the top-performing compounds were less than 1 (average probability of 0.96) (Table 6).

In their toxicity towards the metabolic enzymes, all three compounds were revealed from the predictions to have no toxic effect on these enzymes, except Fostamatinib on CYP2D6, with a probability of 0.63 (Table 6).

Discussions

G-protein-coupled receptor 176 (GPR176) is a member of the orphan human G-protein-coupled receptor 1 family that encodes a glycosylated protein made up of 515 amino acids[17]. GPR176, also known as HB-954 and Gm1012, is characterised by active and inactive conformations that can undergo conformational changes both at the baseline level and in the presence of a ligand, leading to the activation of the heterotrimeric G protein's α subunit, which binds to GTP and subsequently activates the cAMP or phosphatidylinositol signalling pathway, leading to the transmission of extracellular signals[17]. Previous research studies have shown that GPR176 expression is higher in high-grade tumors of diffuse malignant epithelioid mesothelioma, esophageal cancer, gastric cancer, cholangiocarcinoma, colorectal cancer, and other cancers than in normal tissues[17,56,58,58]. The knockdown of GPR176 leads to a reduction in proliferation, migration, and epithelial-mesenchymal transition (EMT) of breast cancer cells[17]. The upregulated expression of G protein-coupled receptors in various cancers has inspired research towards GPCRs to identify the targeting drug against them[59]. Thus, inhibitors of GPR176 could serve as potential drugs for cancer treatment. There are no established drugs that target the GPR176; thus, this study aims to identify potential inhibitors of human GPR176 using computational techniques.

The structural quality assessment confirmed the reliability of the modelled GPR176 protein (Figs. 1 and 14). The Ramachandran, ProSA-web, and the DeepTMHMM analyses provided confidence that the structural features were consistent with the canonical GPCR fold, as misfolded or poorly validated models often lead to inaccurate docking predictions and misinterpretation of ligand interactions[51,54]. For the binding site results, the identification of a binding pocket within the transmembrane helices of GPR176 reveals its viability as a potential therapeutic target. Such binding crevices are often conserved across class A GPCRs[52,53]. The GPR176 binding cavity displayed satisfactory features comparable to pockets characterized in other class A receptors, suggesting a conserved ligand recognition mechanism (61). The composition of hydrophobic and polar residues forming the predicted binding site suggests that GPR176 may accommodate structurally diverse ligands. These findings are consistent with recent studies on establishing orphan GPCRs and ensemble-docking approaches, which showed that predicted binding pockets can reliably guide virtual screening and molecular simulations in the absence of experimental structures[51,53,60]. Overall, these results (Figs. 2 and 3) validate the structural robustness of the GPR176 homology model and provide a foundation for downstream docking simulations.

Based on our docking results, Fostamatinib and Ticagrelor have been identified as novel potential inhibitors of GPR176 (Table 2). Fostamatinib is used clinically for chronic immune thrombocytopenia, while Ticagrelor is used for the prevention of atherothrombotic events (Pantziarka et al., 2018). Previously, Muthiah and associates evaluated the inhibitory potential of FDA-approved anti-cancers to inhibit the GPR 116, and they identified Doxorubicin, Neratinib maleate, Epirubicin, and Lapatinib Ditosylate had good interactions with the protein[59]. In another in silico study of natural compounds with GPR120, it was revealed that silibinin (− 6.87 kcal/mol), withanolide (− 6.19 kcal/mol), limonene (− 6.17 kcal/mol), and cervical (− 6.15 kcal/mol) had good docking interactions with active site residues of the GPR120[61] which are quite lower than the docking scores obtained for Fostamatinib and Ticagrelor. Furthermore, these results were corroborated by the MMGBSA. The binding energies indicated that the approved drugs had good binding tendencies to the GPR176 protein, which suggests that these compounds can cause strong conformational changes in the protein's active site and elicit inhibitory actions on the GPR176.

The Mulliken charge distribution was used to characterize the reactivity and ability of the two top-performing FDA-approved drugs to form intermolecular interactions with the GPR176 protein. The results showed that Fostamatinib and Ticagrelor have a greater tendency to react and form strong interactions with GPR176 than Vismodegib (Fig. 8). This is mainly due to the presence of electron-rich centers, indicated by negative charges, around their atoms. This implies that electrophilic attacks will trigger the reactivity of these compounds at the binding site. These compounds will donate their electrons to interact with the amino acid residues in the

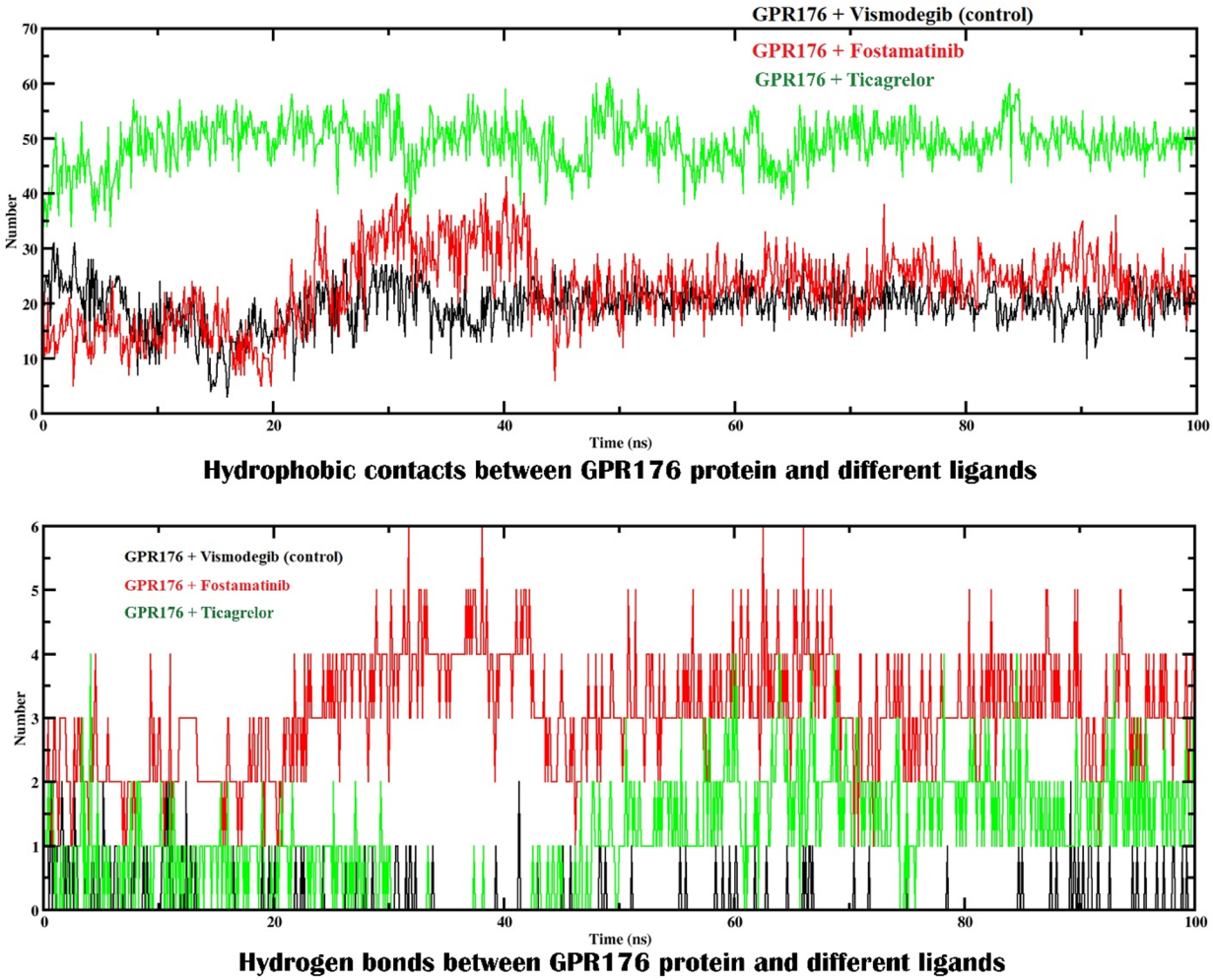

Fig. 14. G-protein coupled receptor 176 in surface presentation.

binding pocket of the GPR176 protein when compared with the control, whose reactions will be attributed to nucleophilic attacks due to its more electron-deficient centres around its atoms (Figs. 5 and 4, and 6).

From the perspective of frontier orbital theory, a broader gap reflects enhanced kinetic stability and reduced likelihood of electronic transitions, thereby limiting overall chemical reactivity. In contrast, smaller gaps facilitate electron transfer processes, making these ligands more chemically "soft" and responsive to external perturbations. Due to this, Fostamatinib and Ticagrelor are susceptible to attracting more electrons. The reduced HOMO–LUMO separation in Fostamatinib (5.79 eV) and Ticagrelor (5.32 eV) suggests that these compounds possess higher polarizability and adaptability within the GPR176 binding crevice (Fig. 8). Whereas, Vismodegib's larger gap (6.47 eV) is consistent with a more rigid and electronically inert profile within the GPR176 binding pocket (Fig. 8).

The conclusions from the frontier orbital theory were corroborated by the calculations of the Global reactivity descriptors. Within the framework of conceptual DFT, hardness reflects a molecule's resistance to changes in its electron density, while softness represents its polarizability and ease of charge redistribution. Accordingly, the lower hardness values of Fostamatinib and Ticagrelor imply that these ligands are more chemically adaptable and reactive, whereas Vismodegib retains a comparatively rigid, "hard" electronic nature (Table 4). The chemical potential (μ), defined as the negative of electronegativity, provides insight into the electron-donating or -accepting tendency of the compounds. When μ is combined with η, it yields the electrophilicity index ($\omega = \mu^2/2\eta$), where larger values correspond to a stronger ability to accept electron density. In this context, Fostamatinib and Ticagrelor are predicted to have higher ω values than Vismodegib, indicating the capacity to stabilize additional charge during receptor binding (Table 4).

The RMSD estimates the differences in the average distances between the core structure of the proteins and their structures under simulations. The results revealed that, out of the three complexes, the Fostamatinib-GPR176 complex was the most rigid. The complex had lower RMSD values compared to the Ticagrelor-GPR176 and Vismodegib-GPR176 complexes. This implies that Fostamitinib, when bound to the GPR176 protein, confers stability: a high tendency that the molecular interactions at the binding sites are robust, reliable, and sturdy, in comparison with the control-bound complex with higher deviations (Figure. 10). This signifies that

Classification	Target	Fostamatinib		Ticagrelor		Vismodegib	
		Prediction	Probability	Prediction	Probability	Prediction	Probability
Organ toxicity	Hepatotoxicity	Inactive	0.73	Active	0.52	Inactive	0.50
	Neurotoxicity	Active	0.59	Inactive	0.77	Inactive	0.81
	Nephrotoxicity	Inactive	0.60	Active	0.67	Inactive	0.63
	Respiratory toxicity	Active	0.86	Active	0.95	Active	0.86
	Cardiotoxicity	Inactive	0.75	Inactive	0.72	Inactive	0.83
Toxicity endpoints	Carcinogenicity	Inactive	0.61	Inactive	0.50	Inactive	0.66
	Immunotoxicity	Inactive	0.78	Active	0.89	Inactive	0.69
	Mutagenicity	Inactive	0.57	Active	0.50	Inactive	0.83
	Cytotoxicity	Inactive	0.51	Inactive	0.67	Inactive	0.71
	BBB-barrier	Active	0.77	Active	0.51	Active	0.87
	Ecotoxicity	Active	0.57	Inactive	0.52	Inactive	0.67
	Clinical toxicity	Active	0.67	Active	0.55	Active	0.64
	Nutritional toxicity	Inactive	0.70	Inactive	0.63	Inactive	0.53
Tox21-Nuclear receptor signalling pathways	Aryl hydrocarbon Receptor (AhR)	Inactive	0.76	Inactive	0.81	Inactive	0.90
	Androgen Receptor (AR)	Inactive	0.93	Inactive	0.96	Inactive	0.99
	Androgen Receptor Ligand Binding Domain (AR-LBD)	Inactive	0.95	Inactive	0.94	Inactive	0.99
	Aromatase	Inactive	0.87	Inactive	0.82	Inactive	0.91
	Estrogen Receptor Alpha (ER)	Inactive	0.84	Inactive	0.84	Inactive	0.89
	Estrogen Receptor Ligand Binding Domain (ER-LBD)	Inactive	0.95	Inactive	0.94	Inactive	0.97
	Peroxisome Proliferator Activated Receptor Gamma (PPAR-Gamma)	Inactive	0.98	Inactive	0.78	Inactive	0.95
	Nuclear factor (erythroid-derived 2)-like 2/antioxidant responsive element (nrf2/ARE)	Inactive	0.93	Inactive	0.92	Inactive	0.96
	Heat shock factor response element (HSE)	Inactive	0.93	Inactive	0.92	Inactive	0.96
	Mitochondrial Membrane Potential (MMP)	Inactive	0.73	Inactive	0.67	Inactive	0.60
	Phosphoprotein (Tumor Supressor) p53	Inactive	0.80	Inactive	0.84	Inactive	0.88
	ATPase family AAA domain-containing protein 5 (ATAD5)	Inactive	0.94	Inactive	0.88	Inactive	0.94
Molecular Initiating Events	Thyroid hormone receptor alpha (THRα)	Inactive	0.90	Inactive	0.85	Inactive	0.86
	Thyroid hormone receptor beta (THRβ)	Inactive	0.78	Inactive	0.66	Inactive	0.53
	Transtyretrin (TTR)	Inactive	0.97	Inactive	0.76	Inactive	0.65
	Ryanodine receptor (RYR)	Inactive	0.98	Inactive	0.76	Inactive	0.96
	GABA receptor (GABAR)	Inactive	0.96	Inactive	0.70	Inactive	0.96
	Glutamate N-methyl-D-aspartate receptor (NMDAR)	Inactive	0.92	Inactive	0.89	Inactive	0.98
	alpha-amino-3-hydroxy-5-methyl-4-isoxazolepropionate receptor (AMPAR)	Inactive	0.97	Inactive	0.89	Inactive	1
	Kainate receptor (KAR)	Inactive	0.99	Inactive	0.98	Inactive	1
	Achetylcholinesterase (AChE)	Inactive	0.73	Inactive	0.62	Inactive	0.96
	Constitutive androstane receptor (CAR)	Inactive	0.98	Inactive	0.99	Inactive	0.99
	Pregnane X receptor (PXR)	Inactive	0.92	Inactive	0.68	Active	0.51
	NADH-quinone oxidoreductase (NADHOX)	Inactive	0.97	Inactive	0.90	Inactive	0.97
	Voltage gated sodium channel (VGSC)	Inactive	0.95	Inactive	0.66	Inactive	0.6
	Na+/I- symporter (NIS)	Inactive	0.98	Inactive	0.79	Inactive	0.93
Metabolism	Cytochrome CYP1A2	Inactive	0.87	Inactive	0.84	Inactive	0.71
	Cytochrome CYP2C19	Inactive	0.77	Inactive	0.79	Inactive	0.63
	Cytochrome CYP2C9	Inactive	0.65	Inactive	0.66	Active	0.65
	Cytochrome CYP2D6	Active	0.63	Inactive	0.63	Inactive	0.73
	Cytochrome CYP3A4	Inactive	0.79	Inactive	0.66	Inactive	0.50
	Cytochrome CYP2E1	Inactive	0.98	Inactive	0.97	Inactive	1

Table 6. Pro Tox 3.0 prediction of oral toxicity for Fostamatinib, Ticagrelor, and vismedogib (control).

the molecular interactions within the complex, at the binding site, are largely unstable and not reliable. For the RMSF, we implemented this procedure to evaluate the flexibility and dynamic behavior of individual amino acid residues at the binding crevice. We observed that the situation of the Fostamatinib and Ticagrelor at the binding crevice of the GPR176 protein stabilized the protein fluctuations, with Fostamatinib exhibiting the highest reduction in fluctuations, followed by Ticagrelor, compared with the Vismodegib (Figure. 11). This implies that

the binding of Fostamatinib at the binding crevice would trigger more stability, thus, less random motion of the proteins, which will strengthen the intermolecular interactions of Fostamatinib to elicit conformational change in the GPR176 protein.

The radius of gyration trajectory was retrieved to characterize the impact of these drug molecules on the compactness and conformational flexibility of the protein structure. Even with the fact that the results indicate that the Fostamatinib-GPR176 complex had a lower gyration profile, in numerical terms. The impact of this difference is negligible as all ligand–protein systems display overall globular conformations without evidence of large-scale unfolding. This implies that there is minimal change in GPR176 structure upon the binding of the Fostamtinib and Ticagrelor at the binding crevice (Fig. 11). The Ligand-Receptor distance generates insights specific to the drug-target interactions. From the results, it was revealed that all three complexes had stable binding with negligible fluctuations occurring at the binding pocket of the GPR176 when all three tested compounds are bound to the protein.

Overall, Fostamatinib demonstrates the greatest ability to stabilize the structural dynamics of GPR176. It is associated with the lowest RMSD and RMSF values, indicating reduced conformational flexibility, and also promotes a slight compaction of the receptor as reflected by lower Rg values compared with the apo form. In addition, Fostamatinib consistently forms several hydrogen bonds along with moderate hydrophobic interactions, highlighting a strong and balanced binding pattern (Figs. 12 and 13). In contrast, Ticagrelor achieves the closest ligand–receptor proximity and the largest number of hydrophobic contacts, but this comes with higher RMSD values and localized flexibility, suggesting a less stabilizing effect. The control compound Vismodegib presents intermediate behavior across these parameters (Fig. 12). Collectively, these results indicate that Fostamatinib provides the most stable and specific GPR176 complex, whereas Ticagrelor's interaction is primarily hydrophobic with limited impact on overall conformational stability (Fig. 12).

Fostamatinib and Ticagrelor present somewhat opposite ADME profiles: fostamatinib is a large, highly polar prodrug (to an active moiety) with low lipophilicity and very limited solubility, while Ticagrelor is smaller, more lipophilic, yet still sparingly soluble (Table 5). Both suffer from low oral bioavailability risks (high PSA, P-gp efflux), and neither penetrates the CNS. Ticagrelor's higher lipophilicity may facilitate cell membrane permeation (reflected in its measurable bioavailability of ~ 36% despite predictions of "low absorption"), while fostamatinib relies on enzymatic conversion (intestinal phosphatases) to its active form. Metabolically, both engage CYP3A4 (as inhibitors and substrates), so drug interactions via CYP3A4 are important in each case. From a drug-development perspective, Ticagrelor's more balanced properties (no Lipinski violations, moderate absorption despite low solubility) have aided its success as an oral antiplatelet, while fostamatinib's extreme polarity and size pose challenges (solubility, absorption) that must be addressed via formulation (it is given as a disodium prodrug salt) and by accepting it as a high-PSA molecule. For their toxicology profile, it was revealed that Fostamatinib was relatively safe; the compound is predicted to belong to Class V for toxic compounds. They have a lower tendency to be harmful to the administration. On the contrary, Ticagrelor was pointed to be potentially toxic, predicted to belong to Class II when compared with the control (Vismodegib). This implies that Fostamatinib will exhibit a similar safety profile to Vismodegib, while Ticagrelor showed a higher toxicity. In affecting the nuclear receptor signaling pathways and Molecular Initiating events, these compounds pose no risk and, as such, have a strong likelihood of not initiating a specific type of toxicity mediated by these receptors. All three compounds revealed no toxicity on the metabolic enzymes; the implication is that Fostamatinib and Ticagrelor possess low potential for acute toxicity and have no tendency to interfere with the core cellular functions and energy production pathways. With this, we recommend the modification of the chemo similar to these two compounds, for the improvement of their toxicological properties while retaining or having an improvement in their binding affinities. Overall, Ticagrelor shows more "drug-like" ADME characteristics, while fostamatinib's atypical profile (large polar prodrug) requires careful handling but is manageable with specialized formulations (Table 5).

It is appropriate to acknowledge the inherent limits of the current work, as it is purely computer-driven research. However, fostamatinib and Ticagrelor show promise against GPR176. The GRP176 model used was a theoretical prediction despite being validated and reliable. There is some level of uncertainty compared to a crystal or cryo-EM resolved structure. Finally, our simulations present a simple view of the complex conformational landscape of GPCRs, although informative. Another key limitation is that the MD simulation was conducted under a solvated system devoid of an explicit lipid bilayer. Considering that GPR176 is a transmembrane GPCR which it is been modulated naturally by its membrane surroundings, a next step that involves all-atom MD simulations of both ligand-GPR176 complexes immersed in an explicit phospholipid bilayer may produce higher fidelity prediction before progressing to expensive wet-lab experiments. To ultimately confirm the activity of these FDA-approved drugs against GPR176, techniques such as Surface Plasmon Resonance (SPR) for in vitro binding assay, and confirmation of cAMP accumulation in GPR176-expressed cell lines, and anti-tumor evaluations of both drugs in relevant animal models where GPR176 is overexpressed. We believe these may pave an accelerated path for their clinical evaluations as novel onco-therapeutics, taking advantage of a drug repurposing strategy.

Conclusions

This study aimed to identify new GPR176 inhibitors using structural bioinformatics tools by evaluating already FDA-approved drugs. These drug molecules underwent molecular docking simulations, MMGBSA, DFT, and molecular dynamics simulations to find viable compounds that could inhibit and also deorphanize the GPR176 protein, leading to the identification of Fostamatinib and Ticagrelor. These two drugs showed better binding affinities, stability, and reactivity than the control (Vismodegib). Repurposing these medications paves the way for utilizing GPR176 as a potential therapeutic target for chemotherapy. However, we recommend conducting in vitro and in vivo studies to confirm these findings and further explore new GPR176 inhibitors.

	Name of the compound	Fostamatinib	Ticagrelor
Physicochemical properties	Formula	$C_{23}H_{26}FN_6O_9P$	$C_{23}H_{28}F_2N_6O_4S$
	Molecular weight	580.46 g/mol	522.57 g/mol
	Num. arom. heavy atoms	40	36
	Num. arom. heavy atoms	18	15
	Fraction Csp3	0.30	0.57
	Num. rotatable bonds	10	10
	Num. H-bond acceptors	13	10
	Num. H-bond donors	4	4
	Molar Refractivity	141.79	128.22
	TPSA	196.53 Å²	163.74 Å²
Lipophilicity	Log $P_{o/w}$ (iLOGP)	2.53	3.89
	Log $P_{o/w}$ (XLOGP3)	1.61	2.03
	Log $P_{o/w}$ (WLOGP)	3.13	2.66
	Log $P_{o/w}$ (MLOGP)	0.33	1.71
	Log $P_{o/w}$ (SILICOS-IT)	0.65	1.79
	Consensus Log $P_{o/w}$	1.65	2.42
Water solubility	Log *S* (ESOL)	−4.13	−4.01
	Solubility	4.34e-02 mg/ml; 7.48e-05 mol/l	5.14e-02 mg/ml; 9.84e-05 mol/l
	Class	Moderately soluble	Moderately soluble
	Log *S* (Ali)	−5.35	−5.10
	Solubility	2.60e-03 mg/ml; 4.48e-06 mol/l	4.19e-03 mg/ml; 8.01e-06 mol/l
	Class	Moderately soluble	Moderately soluble
	Log *S* (SILICOS-IT)	−6.10	−4.86
	Solubility	4.64e-04 mg/ml; 8.00e-07 mol/l	7.23e-03 mg/ml; 1.38e-05 mol/l
	Class	Poorly soluble	Moderately soluble
Pharmacokinetics	GI absorption	Low	Low
	BBB permeant	No	No
	P-gp substrate	Yes	Yes
	CYP1A2 inhibitor	No	No
	CYP2C19 inhibitor	No	No
	CYP2C9 inhibitor	No	No
	CYP2D6 inhibitor	No	No
	CYP3A4 inhibitor	Yes	Yes
	Log K_p (skin permeation)	−8.70 cm/s	−8.05 cm/s

Table 5. ADME and drug-likeness analysis.

Data availability

All data generated or analyzed during this study are included in this published article.

Received: 15 October 2025; Accepted: 3 December 2025
Published online: 02 January 2026

References

1. Tang, J. et al. GPR176 Promotes Cancer Progression by Interacting with G Protein GNAS to Restrain Cell Mitophagy in Colorectal Cancer. *Adv. Sci.* **10**(12), 2205627. https://doi.org/10.1002/advs.202205627 (2023).
2. Zhang, M. et al. G protein-coupled receptors (GPCRs): advances in structures, mechanisms and drug discovery. *Sig Transduct. Target. Ther.* **9**(1), 88. https://doi.org/10.1038/s41392-024-01803-6 (2024).
3. Wang, T. et al. Identification and functional characterisation of N-linked glycosylation of the orphan G protein-coupled receptor Gpr176. *Sci. Rep.* **10**(1), 4429. https://doi.org/10.1038/s41598-020-61370-y (2020).
4. Alhosaini, K., Azhar, A., Alonazi, A. & Al-Zoghaibi, F. GPCRs: the most promiscuous druggable receptor of the mankind. *Saudi Pharm. J.* **29**(6), 539–551. https://doi.org/10.1016/j.jsps.2021.04.015 (2021).
5. Hilger, D. The role of structural dynamics in GPCR-mediated signaling. *FEBS J.* **288**(8), 2461–2489. https://doi.org/10.1111/febs.15841 (2021).
6. Liccardo, F., Luini, A., Martino, R. D. & G-Proteins, Jan. Endomembrane-based signaling by GPCRs and G-proteins. *Cells* **11**(3), 528. https://doi.org/10.3390/cells11030528 (2022).
7. Sisignano, M., Fischer, M. J. M. & Geisslinger, G. Proton-sensing GPCRs in health and disease. *Cells* **10**(8), 2050. https://doi.org/10.3390/cells10082050 (2021).
8. Thompson, M. D. et al. G protein-coupled receptor (GPCR) gene variants and human genetic disease. *Crit. Rev. Clin. Lab. Sci.* **61**(5), 317–346. https://doi.org/10.1080/10408363.2023.2286606 (2024).
9. Wong, T. S. et al. G protein-coupled receptors in neurodegenerative diseases and psychiatric disorders. *Sig Transduct. Target. Ther.* **8**(1), 177. https://doi.org/10.1038/s41392-023-01427-2 (2023).

10. Monfared, R. V. et al. Transcriptome Profiling of Dysregulated GPCRs Reveals Overlapping Patterns across Psychiatric Disorders and Age-Disease Interactions. *Cells* **10**(11), 2967. https://doi.org/10.3390/cells10112967 (2021).
11. Zeng, Z. et al. Roles of G protein-coupled receptors in inflammatory bowel disease. *World J. Gastroenterol.* **26**(12), 1242–1261. https://doi.org/10.3748/wjg.v26.i12.1242 (2020).
12. Cabral-Marques, O. et al. Autoantibodies targeting GPCRs and RAS-related molecules associate with COVID-19 severity. *Nat. Commun.* **13**(1), 1220. https://doi.org/10.1038/s41467-022-28905-5 (2022).
13. Gad, A. A. & Balenga, N. The Emerging Role of Adhesion GPCRs in Cancer. *ACS Pharmacol. Transl. Sci.* **3**(1), 29–42. https://doi.org/10.1021/acsptsci.9b00093 (2020).
14. Chaudhary, P. K. & Kim, S. An Insight into GPCR and G-Proteins as Cancer Drivers. *Cells* **10**(12), 3288. https://doi.org/10.3390/cells10123288 (2021).
15. Cosín-Roger, J., Ortiz-Masia, D., Barrachina, M. D. & Calatayud, S. Metabolite sensing GPCRs: promising therapeutic targets for cancer treatment?. *Cells* **9**(11), 2345. https://doi.org/10.3390/cells9112345 (2020).
16. Yang, N., Yun, W., Cui, Z. & Zheng, H. The oncogenic roles of GPR176 in ovarian cancer: a molecular target for aggressiveness and gene therapy. *J. Obstet. Gynaecol.* **44**(1), 2347430. https://doi.org/10.1080/01443615.2024.2347430 (2024).
17. Yun, W. et al. Oncogenic roles of GPR176 in breast cancer: a potential marker of aggressiveness and a potential target of gene therapy. *Clin. Transl. Oncol.* **25**(10), 3042–3056. https://doi.org/10.1007/s12094-023-03174-w (2023).
18. Ni, L. et al. GPR176 Is a Biomarker for Predicting Prognosis and Immune Infiltration in Stomach Adenocarcinoma. *Mediators of Inflammation* **1**, 7123568. https://doi.org/10.1155/2023/7123568 (2023).
19. Tang, J. et al. GPR176 Promotes Cancer Progression by Interacting with G Protein GNAS to Restrain Cell Mitophagy in Colorectal Cancer. *Adv. Sci.* https://doi.org/10.1002/advs.202205627 (2023).
20. Berdigaliyev, N. & Aljofan, M. An overview of drug discovery and development. *Future Med. Chem.* **12**(10), 939–947. https://doi.org/10.4155/fmc-2019-0307 (2020).
21. Kiriiri, G. K., Njogu, P. M. & Mwangi, A. N. Exploring different approaches to improve the success of drug discovery and development projects: a review. *Futur J. Pharm. Sci.* **6**(1), 27. https://doi.org/10.1186/s43094-020-00047-9 (2020).
22. Roope, L. S. J. The economic challenges of new drug development. *J. Controlled Release* **345**, 275–277. https://doi.org/10.1016/j.jconrel.2022.03.023 (2022).
23. Bhutani, P. et al. U.S. FDA Approved Drugs from 2015–June 2020: A Perspective. *J. Med. Chem.* **64**(5), 2339–2381. https://doi.org/10.1021/acs.jmedchem.0c01786 (2021).
24. Brown, D. G. & Wobst, H. J. A Decade of FDA-Approved Drugs (2010–2019): Trends and Future Directions. *J. Med. Chem.* **64**(5), 2312–2338. https://doi.org/10.1021/acs.jmedchem.0c01516 (2021).
25. Pantziarka, P. et al. ReDO_DB: the repurposing drugs in oncology database. *Ecancermedicalscience* **12**, 886. https://doi.org/10.3332/ecancer.2018.886 (2018).
26. Sadybekov, A. V. & Katritch, V. Computational approaches streamlining drug discovery. *Nature* https://doi.org/10.1038/s41586-023-05905-z (2023).
27. Umar, H. I. et al. Exploring Plant-Derived Natural Products Against *Plasmodium falciparum* Malaria Causative Agent by Targeting Protein Kinase 5: Insights Into Computational Approaches. *Chem. Biodivers.* e02991. https://doi.org/10.1002/cbdv.202402991 (2025).
28. Lin, X., Li, X. & Lin, X. A Review on Applications of Computational Methods in Drug Screening and Design. *Molecules* **25**(6), 1375. https://doi.org/10.3390/molecules25061375 (2020).
29. Umar, H. I. et al. In Silico Exploration of Anti-Cancer Phytochemicals as Novel Inhibitors of LRRK2 via the WDR Domain, *ChemistrySelect*, vol. 10, no. 42, https://espace.library.uq.edu.au/view/UQ:5229884(2025)
30. Naithani, U. & Guleria, V. Integrative computational approaches for discovery and evaluation of lead compound for drug design. *Front. Drug Discov.* https://doi.org/10.3389/fddsv.2024.1362456 (2024).
31. Umar, H. I. et al. An Integrative Computational Approach for the Identification of C-Abl Kinase Inhibitors from Anti-Parkinson Plant-Derived Bioactive. *MC* **21**(9), 969–986. https://doi.org/10.2174/0115734064310145240822060730 (2025).
32. Ghosh, K. et al. CO2 activation on transition metal decorated graphene quantum dots: An insight from first principles. *Phys. E: Low-dimensional Syst. Nanostruct.* **135**, 114993. https://doi.org/10.1016/j.physe.2021.114993 (2022).
33. Ishabiyi, F. O. et al. In silico Assessment of Phytochemicals from Selected Plants as Prospective TGF-β1 Inhibitors for Prostate Cancer Therapy. *Chem. Select* **9**(40), e202401413. https://doi.org/10.1002/slct.202401413 (2024).
34. Roy, D. J., Singh, S. K., Dutta, T., Pradhan, S. & Sinha, B. Volumetric and viscometric study of caffeine in aqueous D-sorbitol solutions. *J. Chem. Thermodyn.* **204**, 107445. https://doi.org/10.1016/j.jct.2024.107445 (2025).
35. Baby, K. et al. Computational drug repurposing of Akt-1 allosteric inhibitors for non-small cell lung cancer. *Sci. Rep.* **13**, 7947. https://doi.org/10.1038/s41598-023-35122-7 (2023).
36. Temitope, I. et al. Molecular docking analysis of phyto-constituents from Cannabis sativa with pfDHFR. *Bioinformation* **14**(9), 574–579. https://doi.org/10.6026/97320630014574 (2018).
37. Oraibi, A. I., Karav, S. & Khallouki, F. Exploration of Rosmarinic Acid as Anti-Esophageal Cancer Potential by use of Network Pharmacology and Molecular Docking Approaches, *Atlantic Journal of Life Sciences*, vol. no. 1, 2025, Accessed: Apr. 23, https://atjls.com/index.php/home/article/view/7(2025).
38. Gunasekaran, V. & Dhakshinamurthy, S. S. Computational insights into the interaction of pinostrobin with Bcl-2 family proteins: A molecular Docking analysis. *Asian Pac. J. Cancer Prev.* **25** (2), 507–512. https://doi.org/10.31557/APJCP.2024.25.2.507 (2024).
39. Paul, S. et al. Hydrothermal synthesis and characterization of FeSbO2F2 nanoparticle and its applications towards hydrogen evolution reaction, dye management and bacterial disinfection studies. *Inorg. Chem. Commun.* **175**, 114073. https://doi.org/10.1016/j.inoche.2025.114073 (2025).
40. Sánchez-Márquez, J. et al. Introducing 'UCA-FUKUI' software: reactivity-index calculations. *J. Mol. Model.* **20**(11), 2492. https://doi.org/10.1007/s00894-014-2492-1 (2014).
41. Jo, S., Kim, T., Iyer, V. G. & Im, W. CHARMM-GUI: a web-based graphical user interface for CHARMM. *J. Comput. Chem.* **29**(11), 1859–1865. https://doi.org/10.1002/jcc.20945 (2008).
42. Jorgensen, W. L., Chandrasekhar, J., Madura, J. D., Impey, R. W. & Klein, M. L. Comparison of simple potential functions for simulating liquid water. *J. Chem. Phys.* **79**(2), 926–935. https://doi.org/10.1063/1.445869 (1983).
43. Huang, J. & MacKerell, A. D. Jr CHARMM36 all-atom additive protein force field: validation based on comparison to NMR data. *J. Comput. Chem.* **34** (25), 2135–2145. https://doi.org/10.1002/jcc.23354 (2013).
44. Vanommeslaeghe, K. et al. CHARMM general force field: A force field for drug-like molecules compatible with the CHARMM all-atom additive biological force fields. *J. Comput. Chem.* **31** (4), 671–690. https://doi.org/10.1002/jcc.21367 (2010).
45. Abraham, M. J. et al. GROMACS: High performance molecular simulations through multi-level parallelism from laptops to supercomputers. *SoftwareX* **1–2**, 19–25. https://doi.org/10.1016/j.softx.2015.06.001 (2015).
46. Darden, T., York, D. & Pedersen, L. Particle mesh Ewald: An N·log(N) method for Ewald sums in large systems. *J. Chem. Phys.* **98**(12), 10089–10092. https://doi.org/10.1063/1.464397 (1993).
47. Kumari, R., Kumar, R., Lynn, A., High-Throughput, M. M. P. B. S. A. & Calculations g_mmpbsa—A GROMACS Tool for *J. Chem. Inf. Model.*, **54**, 7, 1951–1962, doi: https://doi.org/10.1021/ci500020m.Jul. (2014).
48. Daina, A., Michielin, O. & Zoete, V. SwissADME: a free web tool to evaluate pharmacokinetics, drug-likeness and medicinal chemistry friendliness of small molecules. *Sci. Rep.* https://doi.org/10.1038/srep42717 (2017).

49. Banerjee, P., Kemmler, E., Dunkel, M. & Preissner, R. ProTox 3.0: a webserver for the prediction of toxicity of chemicals. *Nucleic Acids Res.* **52**, W513–W520. https://doi.org/10.1093/nar/gkae303 (2024).
50. Banerjee, P., Eckert, A. O., Schrey, A. K. & Preissner, R. ProTox-II: a webserver for the prediction of toxicity of chemicals. *Nucleic Acids Res.* **46**, W257–W263. https://doi.org/10.1093/nar/gky318 (2018).
51. Szwabowski, G. L. et al. Benchmarking GPCR homology model template selection in combination with de novo loop generation. *J. Comput. Aided Mol. Des.* **34**(10), 1027–1044. https://doi.org/10.1007/s10822-020-00325-x (2020).
52. Lee, S. et al. Evaluating GPCR modeling and docking strategies in the era of deep learning-based protein structure prediction. *Comput. Struct. Biotechnol. J.* **21**, 158–167. https://doi.org/10.1016/j.csbj.2022.11.057 (2023).
53. McKay, K., Hamilton, N. B., Remington, J. M., Schneebeli, S. T. & Li, J. Essential Dynamics Ensemble Docking for Structure-Based GPCR Drug Discovery. *Front. Mol. Biosci.* **9**, https://doi.org/10.3389/fmolb.2022.879212 (2022).
54. Heo, L. & Feig, M. Multi-state modeling of G-protein coupled receptors at experimental accuracy. *Proteins* **90**(11), 1873–1885. https://doi.org/10.1002/prot.26382 (2022).
55. Wang, E. et al. End-Point Binding Free Energy Calculation with MM/PBSA and MM/GBSA: Strategies and Applications in Drug Design. *Chem. Rev.* **119**(16), 9478–9508. https://doi.org/10.1021/acs.chemrev.9b00055 (2019).
56. Forest, F. et al. Histopathological typing in diffuse malignant epithelioid mesothelioma: implication for prognosis and molecular basis. *Pathology* **53**(6), 728–734. https://doi.org/10.1016/j.pathol.2021.01.010 (2021).
57. Gu, X. et al. Exploring the Correlation Between GPR176, a Potential Target Gene of Gastric Cancer, and Immune Cell Infiltration. *Pharmgenomics Pers. Med.* **16**, 519–535. https://doi.org/10.2147/PGPM.S411199 (2023).
58. Shimada, I., Ueda, T., Kofuku, Y., Eddy, M. T. & Wüthrich, K. GPCR drug discovery: integrating solution NMR data with crystal and cryo-EM structures. *Nat. Rev. Drug Discov.* **18**(1), 59–82. https://doi.org/10.1038/nrd.2018.180 (2019).
59. Muthiah, I., Rajendran, K. & Dhanaraj, P. In silico molecular docking and physicochemical property studies on effective phytochemicals targeting GPR116 for breast cancer treatment. *Mol. Cell. Biochem.* **476**(2), 883–896. https://doi.org/10.1007/s11010-020-03953-x (2021).
60. Kim, J. & Choi, C. Orphan GPCRs in Neurodegenerative Disorders: Integrating Structural Biology and Drug Discovery Approaches. *Cur. Issues Molec. Biol.* **46**(10), 11646–11664. https://doi.org/10.3390/cimb46100691 (2024).
61. Chinthakunta, N., Cheemanapalli, S., Chinthakunta, S., Anuradha, C. M. & Chitta, S. K. A new insight into identification of in Silico analysis of natural compounds targeting GPR120. *Netw. Model. Anal. Health Inf. Bioinform.* **7** (1), 8. https://doi.org/10.1007/s13721-018-0166-0 (2018).
62. Agarwal, M. A. et al. Ventricular Arrhythmia in Cancer Patients: Mechanisms, Treatment Strategies and Future Avenues. *Arrhythm Electrophysiol. Rev.* **12**, e16. https://doi.org/10.15420/aer.2023.04 (2023).
63. Essa, H., Wright, D. J., Dobson, R. & Lip, G. Y. H. Chemotherapy-Induced Arrhythmia – Underrecognized and Undertreated. *Am. J. Med.* **134**(10), 1224–1231. https://doi.org/10.1016/j.amjmed.2021.05.026 (2021).

Acknowledgements

The authors acknowledge the Bioinformatics Resources and Applications Facility (BRAF), C-DAC, Pune, India, for providing computational facilities. We wish to acknowledge AICTE IDEA LAB, JIS College of Engineering, Kalyani, Nadia, West Bengal, India, for Infrastructural support. The authors also acknowledge the guidance and mentorship provided by the facilitators of the internship at the Computer-Aided Therapeutic Discovery and Design Laboratory in Akure, Nigeria. The authors would like to extend their appreciation to King Saud University for funding this work through the Ongoing Research Funding program (ORF-2026-77), King Saud University, Riyadh, Saudi Arabia. The authors also extend their appreciation to the Deanship of Scientific Research and Graduate Studies at King Khalid University for funding this work through the Large Research Project under grant number RGP2/715/46.

Author contributions

All the authors read and approved the final manuscript. Felix Oluwasegun Ishabiyi, Omar A. Almohammed, Denekew Temesgen: Conceptualized the study; Prepared the Original draft of the manuscript; Substantively verified the methodology; Project Administration. Tanmoy Duttaa, Mohammed Bourhia, Esmael M. Alyami: Writing the Original draft; Formal analysis; Investigations; Data Curation; and Software. Okoyenta Celestina Onyinye, Olusola Daniel Damola, Leyla Budagova: Writing the Original draft; Investigations; Data Curation; Software. Ridwan Opeyemi Bello and Haruna Isiyaku Umar, Mona Alsolami: Investigations; Resources; Project administration; Reviewing; Supervision.

Funding

King Saud University funded this work through the Ongoing Research Funding program (ORF-2026-77), and King Khalid University funded this work through the Large Research Project under grant number RGP2/715/46.

Declarations

Competing interests

The authors declare no competing interests.

Ethics approval and consent to participate

This study used publicly available data and did not involve human or animal subjects.

Additional information

Supplementary Information The online version contains supplementary material available at https://doi.org/10.1038/s41598-025-31607-9.

Correspondence and requests for materials should be addressed to F.O.I., H.I.U. or D.T.